UNIVERSITY OF OKLAHOMA
GRADUATE COLLEGE

STUDY ON THE USE OF FACEMASK FIBERS FOR SOIL REINFORCEMENT

A THESIS

SUBMITTED TO THE GRADUATE FACULTY

in partial fulfilment of the requirements for the degree of

MASTER OF SCIENCE

By

JAVIER A. CHAVES CAMARGO

Norman, Oklahoma

2023

STUDY ON THE USE OF FACEMASK FIBERS FOR SOIL REINFORCEMENT

A THESIS APPROVED FOR THE

SCHOOL OF CIVIL ENGINEERING AND ENVIRONMENTAL SCIENCE

BY THE COMMITTEE CONSISTING OF

Dr. Kianoosh Hatami, Chair

Dr. Amy Cerato

Dr. Gerald Miller

Dedicado a Desi y Miriam

Abstract

This study investigated the potential application of facemask materials as a sustainable solution for soil reinforcement, with a focus on assessing the influence of facemask fiber attributes on the geotechnical properties of Fiber-Reinforced Soils (FRS). After conducting interface shear tests and tensile strength tests on facemask materials, CUIC triaxial tests were performed on a raw soil and corresponding FRS specimens, incorporating various facemask fiber configurations and geotextile materials for comparison purposes. Results of study indicate that the inclusion of facemask fibers can indeed influence the magnitudes of FRS cohesion and friction angle relative to raw soil values, leading to an increase in the soil shear strength. Specimens with 2.5 x 51 mm-long fibers at a concentration of 1.2 kg/m^3 led to the greatest strength increase measured in this study, with a total shear strength increase of 39.7%. This performance was followed by that of 5.1 mm-wide and 51 mm-long fibers at 0.8 kg/m^3, resulting in a 31.3% improvement in shear strength. Proper addition of facemask fibers with even spread and random orientation in the soil consistently led to increased shear strength in FRS specimens. This increase was evident not only in the overall toughness of the specimens but also in the effective friction angle, showing an improvement of up to 18%. However, it was observed that effective cohesion remained practically unchanged or, in some cases, decreased by as much as 82%. Additionally, the findings indicate that thinner fibers tend to be more effective in the reinforcement process, and the optimal concentration of facemask fibers is closely associated with their aspect ratio.

Acknowledgements

I wish to extend my profound gratitude to the University of Oklahoma for fostering an exceptional academic environment that has significantly contributed to the successful completion of this master's thesis. The university's nurturing community, and the wealth of opportunities it provided have all played pivotal roles in shaping the outcome of this research.

I am particularly indebted to the invaluable guidance and unwavering support provided by my esteemed committee members. Dr. Kianoosh Hatami, Chair of the committee, deserves special recognition for his outstanding mentorship, insightful feedback, and continuous support throughout the years. His expertise and dedication have been instrumental in ensuring the high quality of this work.

I would also like to express my sincere appreciation to the dedicated faculty and fellow PhD candidates who have contributed to my academic growth, such as Dr. Tommy Bounds and Pouria Zare. They have been instrumental in shaping my research and academic journey. Furthermore, my gratitude extends to Dolese Bros. Co. for generously providing the essential materials required for this research.

Lastly, my family has been an unwavering source of support and motivation. To my mother, father, sister, uncle Desi, and aunt Miriam, I am deeply thankful for your enduring encouragement and love, which have been the foundation of my success in this academic endeavor.

Table of contents

List of Tables

List of Figures

Chapter 1 – Introduction

1.1 Background

Soil reinforcement using stable fibers has been shown to be a viable and economical method to improve the mechanical properties of soils, especially in stabilizing slopes and embankments against shallow failure (Gregory, 2006). Wu et al. (2022) reported that the fiber-reinforced soil (FRS) retrofitting technique can improve a wide range of soil properties including shear, compressive and tensile strengths, liquefaction resistance, foundation bearing capacity, and shrink-swell behavior that otherwise could lead to cracking and structural problems. Consequently, FRS has been used in a wide variety of civil engineering projects, such as retaining walls, slopes, highways, dams, and railway subgrades (Ehrlich, 2019).

FRS is especially useful for fine-grained soils in geographical areas like Oklahoma where such soil types are prevalent. Most of the studies on fine-grained soil have involved the use of thermoplastic polymers (e.g., polypropylene) and experiments that primarily involved triaxial compression tests (Correia, 2021). Meanwhile, several studies have been reported on the use of recycled materials as reinforcement elements (e.g., Ghiassian et al.,2004; Yarbasi, 2016; Jaramillo et al., 2022). Those studies involved the use of recycled tires and carpet waste, as well as bio-based materials such as plant roots, among other materials, and showed that recycled fiber reinforcement can indeed improve soil properties. Therefore, recycled materials upon further investigation could serve as an economical alternative to industrial fibers for FRS applications.

Figure 1 illustrates the composition of a single-use facemask, showing how it is made of three layers of polypropylene. According to the manufacturer (StringKing 2021), the middle layer is melt-blown, while the inner and outer layers are spun bound. Considering that the same material (i.e. polypropylene) is predominantly used to produce conventional FRS fibers, evaluating the suitability of facemask materials for FRS applications would provide further literature related to the recycling of materials, while also addressing environmental pollution concerns. It has been estimated that plastic waste related to medical activities has increased by 340% following the global COVID-19 pandemic in 2020, and a significant quantity of microplastic particles have been released into the environment ever since (Dissanayake, 2021). The specific objective of this study was to investigate the possibility of using shredded recycled facemasks as reinforcement in FRS applications.

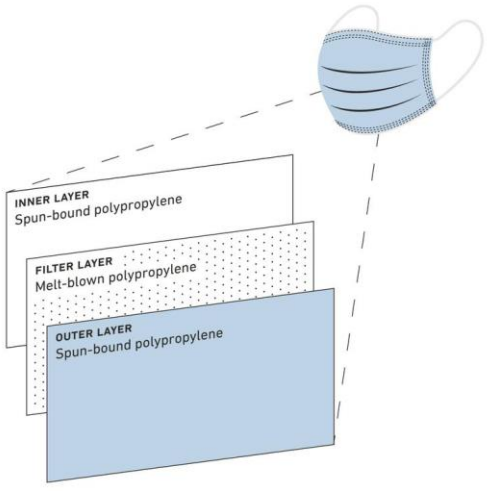

Figure 1: Materials used on each layer of a standard disposable facemask (StringKing 2021)

1.2 Hypotheses and Objectives

The hypotheses of this study included:

1. The shear strength of FRS specimens that include shredded facemasks is greater than that of the otherwise unreinforced (raw) soil.
2. The magnitude of expected improvement in shear strength is a function of the facemask strips' concentration, length and aspect ratio in FRS samples.
3. Improvement in shear strength of the FRS samples can be maximized by using an optimal combination of the strips' concentration, length and aspect ratio in the FRS samples.

The objectives of the conducted study were:

1. Develop a methodology for specimen preparation, setup, and testing of FRS specimens involving shredded facemasks,
2. Assess the feasibility of using shredded facemasks as reinforcement in FRS applications through triaxial tests to determine and quantify improvements in shear strength of FRS relative to that of the comparable raw soil,
3. Quantify the influences of shredded strip length, aspect ratio and concentration on FRS shear strength relative to that of the comparable raw soil.

To the best of the author's knowledge, this is the first study that has examined the feasibility of using shredded facemasks as fiber reinforcement in FRS applications. Results of the study are expected to provide design factors that could be applied to shear strength properties of the raw soil to determine the enhanced properties of the

corresponding FRS specimens for field applications. Another important aspect of the study was to provide an engineering application for waste materials that have been produced in enormous quantities over the last few years and reduce their adverse environmental impact.

1.3 Thesis Organization

This thesis comprises 9 chapters as described below:

Chapter 1 This chapter serves as an introduction, setting the stage for the research study and providing the necessary context for understanding its significance. It outlines the research problem, objectives, and research questions, highlighting the gaps in existing knowledge that the study seeks to address.

Chapter 2 This chapter delves into a literature review that examines existing research and scholarly works related to the study's topic. This chapter establishes the foundation for the research, identifies areas of further investigation, and contributes to the overall theoretical framework of the study.

Chapter 3 This chapter provides an in-depth exploration of the theoretical framework and constructs used to understand fiber materials and fiber-reinforcement of soil. It offers a comprehensive overview of the key

concepts, relationships, and assumptions that form the foundation of the research.

Chapter 4 This chapter provides a comprehensive overview of the materials and equipment used, experimental setup, and the testing procedure employed in the study. It also presents results of preliminary tests conducted on different soils to select a suitable choice for this study.

Chapter 5 This chapter presents the results of the tests conducted on the facemask materials that were used to produce reinforcement fibers. It includes estimations of their tensile strength and their coefficient of interaction with the soil materials.

Chapter 6 This thesis chapter presents the results of Consolidated Undrained Isotropic Compression (CUIC) Triaxial Tests. It encompasses an overview of the conducted tests and an analysis of the mechanical properties measured for each specimen.

Chapter 7 This chapter focuses on analyzing the results in relation to the study's hypothesis and objectives. It encompasses further observations from data presented in the previous chapter.

Chapter 8 This chapters serves as a conclusion of the thesis, presenting a summary of the major findings, and future work recommendations.

Chapter 2 – Literature Review

2.1 Studies on FRS using different soils

Lin and Zornberg (2019) carried out consolidated undrained isotropic compression (CUIC) triaxial tests on sandy soils and examined the effects of soil density, fiber content and fiber length on the stress-strain behavior of the specimens. They reported that adding fibers to the soil consistently increased their shear strength to varying degrees as a function of the factors examined in their study. Similar findings have been reported in several other studies (e.g., Gray and Ohashi 1983; Gray and Al-Refeai 1986; Maher and Gray 1990; Morel and Gourc 1997; Consoli et al. 1998, 2002, 2003, 2004; Zornberg 2002; and Michalowski and Cermák 2003).

Correia (2021) stated that most studies on FRS had focused on sands. As a result, mechanical performance of fiber-reinforced clays was less understood. The paucity of related literature was attributed to a greater difficulty and time requirements for testing clays relative to sands. However, a careful review of related literature indicates that the FRS technology involving clays has been the subject of several studies.

Feuerharmel (2000) carried out consolidated drained (CD) triaxial compression tests on clayey soils reinforced with polypropylene fibers and found that adding 12 mm-long and 36 mm-long fibers increased the soil cohesion by factors of 3 and 5, respectively. However, no detectable change was observed in the soil friction angle. Trindade (2006) carried out similar tests on polypropylene-reinforced clayey soils using 20 mm-long fibers and found that the soil cohesion increased by 70%, with little increase in its friction angle.

Gregory (2006) carried out triaxial tests on both sands and clays. Nevertheless, the time differences reported for the tests in these two categories confirmed that the tests on clays did take longer to set up and complete, to the extent that the shearing stages of clay specimens collectively took ten times as long to complete as those for sand specimens. Table 1 shows a comparison of time durations required to complete triaxial tests on different types of soil as reported by Gregory (2006).

Table 1: Comparison of test durations (in hours) for clay vs. sand specimens (Gregory 2006)

		Clay	
Activity	**No. Specimens**	**Unit Time-Hr**	**Total Time - Hours**
Standard Proctor	10	2	20
Percent < No. 200 Sieve	2	2	4
Liquid-Plastic Limits	4	2	8
Triaxial Spec. Prep	27	26	702
Triaxial Saturation	27	30	810
Triaxial Consol.	27	24	648
Triaxial Shear	27	29	783
Direct Shear Prep	18	26	468
Direct Shear Consol	18	24	432
Direct Shear-Shear	18	23	414
Creep Test Prep	6	26	156
Creep-Shear	6	504	3024
		Sand	
Relative Density	8	2	16
Sieve Analysis	2	2	4
Triaxial Prep	27	3	81
Triaxial Shear	27	1	27
Direct Shear Prep	24	3	72
Direct Shear-Shear	24	1	24
Totals	**Clay and Sand**		**7693**

2.2 ASTM Standard for CUIC Triaxial Testing

ASTM D4767-11 provides a standard method for CUIC testing of cohesive soils, which involves the following steps:

Initially, a cylindrical soil specimen is carefully prepared by trimming and shaping it to the desired dimensions. The specimen is then placed inside a triaxial cell, confining the sample using a rubber membrane, and attaching measurement devices to record axial stress, axial strain, and pore pressure. The soil is then saturated with water, ensuring complete removal of air from void space by applying back pressure to force water into it. After saturation, the specimen undergoes a consolidation process where it is subjected to a confining pressure that forces excess pore water to be expelled. For shearing, an axial load is gradually applied at a rate of 0.5 mm/min to the specimen using a loading device, while measurements of stress, strain, and pore pressure are continuously recorded. The test is continued until the specimen reaches failure, indicated by a significant drop in axial stress or excessive deformation, or a desired strain level. At this point, the test is terminated, and the maximum axial stress and corresponding strain values are recorded.

2.3 Specimen Size Considerations

The ASTM D4767-11 test standard requires a minimum diameter of 33 mm (1.3 inch) and a height-to-diameter ratio (h/d) value of 2 for the cylindrical specimens. Omar (2013) conducted tests on loose sand using different specimen diameters of 38 mm, 50 mm and 70 mm. He reported that larger specimens showed a stiffer behavior during isotropic compression. In a later study, Park and Jeong (2015) compared sand specimens of 50 mm

and 100 mm diameters in both drained and undrained conditions. In the case of undrained conditions, tests on smaller specimens recorded higher friction angles by as much as 2.6°. After comparing their results to other studies on similar sandy soils, they concluded that triaxial testing on sandy soils should be conducted on larger specimens for more accurate results.

2.4 Saturation in CUIC Triaxial Tests

ASTM D4767-11 requires that saturation of specimens must be done such that the voids in the soil are filled with water without prestressing the specimen or allowing it to swell. An important consideration at this stage is a parameter called the B-value (Figure 2), which measures to what degree changes in cell pressure are resisted by the water in the specimen, rather than the soil. This is calculated by temporarily increasing the confining pressure in the triaxial chamber, dividing the change in pore water pressure by the change in confining pressure (u/σ_3). Saturation is determined as practically complete once the B-value of the specimen reaches 0.95 or higher.

Sugiyama et al. (2016) studied the effects of stress conditions and stress history on B-values in triaxial testing of kaolin clay soils. They carried out experiments and numerical simulations on highly saturated specimens to investigate the behaviors of air and water when subjected to different back pressures, ranging from 100 to 500 kPa. They concluded that high initial back pressures together with small initial effective stresses needed to be used at the start of B-value measurements to increase the sensitivity of the pore water pressure response in CUIC triaxial testing of clays.

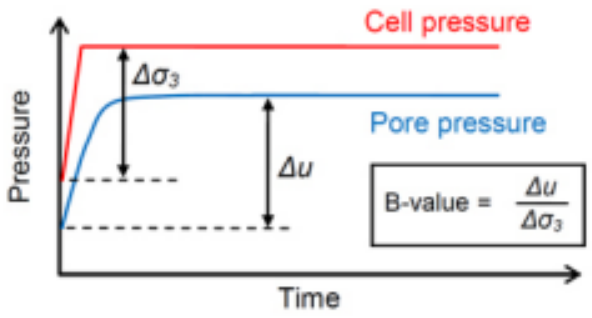

Figure 2: Schematic of B-value check process

Additionally, it was noted that B-value measurement cycles create a stress history on the specimen that affects the accuracy of future measurements, leading to less accurate estimations of saturation if the B-value check is conducted too frequently. The ASTM standard does not indicate a range of desirable back pressure values for the saturation stage. Therefore, the above study suggests that high back pressure values are desirable in order to decrease the time required to complete this process and obtain more accurate B-value readings. Figure 3 from the corresponding ASTM standard shows the degree of saturation as a function of back pressure.

Lowe and Johnson (1960) conducted studies on the effect of saturation on the measured shear strength of sandy clay and silty sand soils in CUIC triaxial tests and obtained degrees of saturation above 98% within 2.5 days using back pressures between 100 and 200 psi (690 and 1380 kPa). Consequently, saturation pressures used in this study were kept within the ranges recommended above so that the specimens would reach saturation in a comparable amount of time.

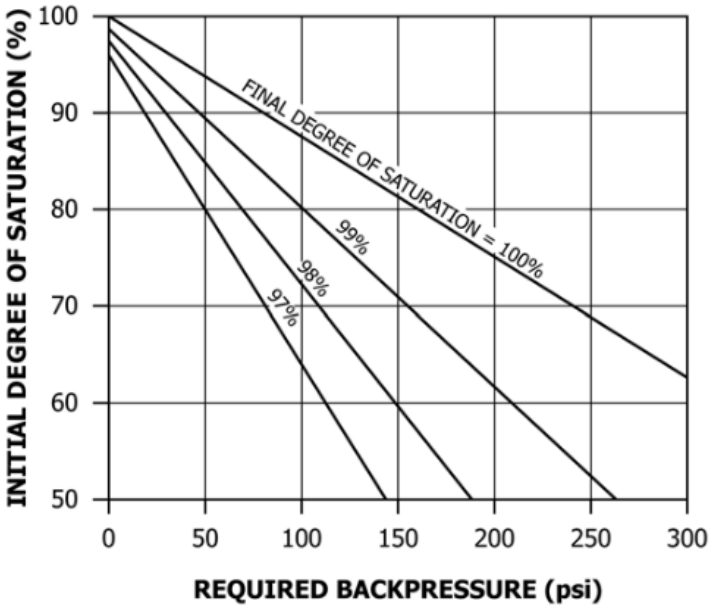

Figure 3: Back Pressure necessary to obtain target degrees of saturation (ASTM D4767)

2.5 Multistage Triaxial Testing

Multistage triaxial testing is a laboratory technique used to simulate the effects of repeated loading and unloading conditions on soils. It involves subjecting a single soil sample to a sequence of consolidation and shearing stages, allowing for the measurement of soil behavior under fluctuating loading conditions. Rivera-Hernandez et al. (2021) conducted single stage and multistage triaxial tests on silty sand samples. The results of both approaches showed sufficient correlation for them to conclude that the use of multistage testing allowed for "reasonable replication of field conditions (e.g., flood loading and unloading) in the laboratory." Nambiar et al. (1985) evaluated the suitability of multistage triaxial testing for testing of marine soils and concluded that, in order to obtain good correspondence with single-stage shearing, multistage shearing must not be done to failure

but up to within 2% to 4% axial strain, and that failure conditions could then be predicted using Kondner's hyperbolic criterion. Soranzo (1988) conducted both unconsolidated undrained (UUIC) and CUIC triaxial tests to compare multistage and single-stage shearing of normally consolidated clays. Reaching axial strains between 8% and 10% at each stage, he concluded that multistage triaxial results were "highly comparable to those of traditional (single stage) triaxial tests," while also providing a time-efficient approach for the evaluation of shearing properties of soils. Consequently, triaxial tests conducted in this study were done using the multi-stage approach in order to maximize the amount of samples that could be tested within the time available for the study.

2.6 Mixing techniques for the fibers and related considerations

Consoli (2006) reported that mixing soils and fibers randomly leads to better shear performance than when they are intentionally placed in a given orientation. The fibers provide reinforcement by acting in tension regardless of the soil sample being subjected to compressive forces, and random mixing with the soil avoided the potential creation of weak planes and early failure. This suggests that the quality of mixing of fibers should be such that it would lead to a random orientation of fibers to maximize the reinforcement potential of the recycled fibers. Studies by Correia (2021) have also shown that if fibers all end up in the same orientation when mixed with the soil, they can lead to increased anisotropy and formation of potential weak planes in the soil. Therefore, it is recommended that fibers should be blended with soil in such a way that while their distribution in soil is practically uniform, they are placed in random orientations (see Sections 4.3.2 and 4.3.3). In a study conducted by Gregory (2006) on FRS specimens involving sands and clays, a

technique for mixing the soil and fibers was recommended. The proposed method suggests that more accurate test results can be achieved by individually mixing fibers with the soil for each test specimen, rather than in larger quantities in the laboratory. This approach allows for visual inspection, ensuring the even distribution of fibers at each level within the soil before mixing and compacting. To maintain accuracy, both the fibers and the soil should be weighed to obtain precise concentrations for each specimen. In Gregory's experiments, manual mixing was performed by kneading the materials until a visually uniform blend was achieved (Figure 4). The resulting reinforced soil specimen was then placed in a zip-lock bag and stored until triaxial testing. Following a similar method, the specimens in this study were prepared using a fine-grained soil and fibers made from shredded facemasks. In this study, the term 'fiber' has been used as a generic term to describe the shredded pieces of polymer that were obtained from commercially available facemasks regardless of their geometric attributes to maintain consistency with the FRS terminology.

Figure 4: Mixing of polymer fibers and soil to prepare individual FRS specimens (Gregory 2006)

2.7 Alternative materials for soil reinforcement

As environmental concerns continue to increase on a global scale, significant research has focused on incorporating recycled and alternative materials to improve sustainability and reduce environmental impact. In the case of FRS, a limited amount of research has been reported on the use of recycled materials for soil reinforcement as an alternative to geosynthetic fibers. Jaramillo et al. (2022) studied the mechanical behavior of clayey soils reinforced with recycled tire rubber. They concluded that recycled fibers helped improve interfacial bonding and overall mechanical behavior, while providing a practical method to recycle waste tires and similar rubber-based materials. Yarbasi (2016) studied the effects of freezing and thawing on clayey soils that were reinforced with strips of scrap tire and observed that FRS specimens made using such recycled materials showed 32.9% lower unconfined compressive strength after they had been frozen at -21 ^{o}C for 28 days, compared to specimens that had not been frozen. Yarbasi's experience indicates that not all recycled materials may serve as products for engineering applications. This notion was kept in mind while examining the suitability of shredded face masks for FRS applications in this study. Table 2 provides a summary of studies on the mechanical behavior of FRS using different recycled materials.

Table 2: Studies on FRS using different recycled materials

Study	Soil Type	Reinforcement Material	Test Method*
Sobhan et al. (2002)	Soil-cement-fly-ash composite	Recycled Polyethylene Strips	Split Tensile Test
Ghiassian et al. (2004)	Clay	Fibrous carpet waste	CDIC Triaxial Test
Yarbasi (2016)	Clayey Soil	Scrap Tires	UCT
Zhang et al. (2018)	Sand	Recycled rubber tire	UCT
Ji (2019)	Clayey Soil	Bermudagrass Root	CUIC Triaxial Test
Soltani et al. (2019)	Expansive Soils	Recycled tire rubber	UCT
Zhou et al. (2019)	Clay	Plant roots	UUIC Triaxial Test
Choobbasti (2019)	Clay mixed with calcium carbonate	Carpet Waste Fibers	UUIC Triaxial Test
Karimdazeh et al. (2021)	Sand	Vetiver grass roots	CUIC Triaxial Test
Jaramillo et al. (2022)	Clayey Soil	Tires as chips and fibers	CDIC Triaxial Test
Rasouli et al. (2022)	Sand	Recycled polypropylene tufted carpet	CUIC Triaxial Test

* CDIC = Consolidated Drained Isotropic Compression
CUIC= Consolidated Undrained Isotropic Compression,
UUIC= Unconsolidated Undrained Isotropic Compression,
UCT= Unconfined Compression Test

2.8 Tensile Properties of Fibers Materials

ASTM D4632 is a standard test method for evaluating the grab breaking load and elongation properties of geotextiles. The test involves preparing representative samples of the geotextile, mounting them securely in a grab testing apparatus, and subjecting them to a preloading period. The samples are then subjected to a gradually increasing tensile load until they break, while the applied force and elongation are measured. The grab breaking load is calculated by dividing the maximum force applied by the sample width, and the elongation is determined as a percentage of the original gauge length. The results are reported in a comprehensive format, including sample details, testing conditions, measured data, and calculations.

2.9 Interface Interaction of Fibers in Soil

ASTM D5321 outlines a test method to determine the shear resistance between a geosynthetic material and soil (or other user-selected materials such as facemask fibers). The test involves placing the soil and the chosen contact material within a direct shear box. A constant normal force is applied to the specimen from the top of the shear box. Simultaneously, a shear force is applied to make one section of the shear box move relative to the other. The shear force is measured as a function of the horizontal displacement of the moving section of the shear box. This test is conducted at a minimum of three different normal stresses. The resulting shear stress values are plotted against the applied normal compressive stresses used in the testing. The test data is typically represented by a linear relationship, with the slope of the line indicating the coefficient of friction between the two materials where shearing occurred. The y-intercept of this line

represents adhesion between the materials.

Figure 5: Setup for interface shear tests by Esmaili (2014)

Figure 5 illustrates the setup used by Esmaili (2014), who conducted this interface shear tests using the equipment available in room S11 of Carson Engineering Center. A geotextile sample was placed on top of the lower half of the shear box, using glue to adhere it to a metallic plate below it and prevent any slipping of the geotextile. Then, the upper half of the cell was placed on top and 4 layers of 3 mm thickness of Chickasaw clay were compacted on top. This setup was replicated in this study for determining the interface interaction of facemask reinforcement elements.

Chapter 3 – Conceptual Model

The increased shear strength of fiber-reinforced soil is believed to be attributed to various mechanisms. These mechanisms include (Gregory 2006, Esmaili 2014):

1. Pullout Resistance: It arises from the frictional interaction between individual fibers and the surrounding soil. As the soil shears, the fibers resist being pulled out, contributing to enhanced shear strength.
2. Adhesion: In cohesive-type soil, adhesion between individual fibers and the surrounding soil further enhances the shear strength. This adhesive interaction helps to increase the resistance to shearing.
3. Micro-Bearing Capacity: During the pullout resistance of individual fibers that are looped across the shear plane, the soil experiences an increased micro-bearing capacity. This additional capacity contributes to the overall shear strength improvement.
4. Increased Localized Normal Stress: The pullout resistance of fibers during soil shearing results in an increased localized normal stress across the shear surface. This additional stress contributes to the overall shear strength enhancement.

These mechanisms collectively contribute to the improved shear strength observed in fiber-reinforced soil.

3.1 Stress Conditions of Fibers in FRS

According to Gregory (2006), assuming a random distribution of fiber orientations with equal probabilities for vertical, horizontal, and intermediate orientations, the effective normal stress along the longitudinal axis of the fiber becomes the average of the vertical and horizontal stresses (Figure 6). Additionally, for fibers with a rectangular cross-section, there is an equal probability of any orientation between vertical and horizontal with respect to the cross-sectional axis. Consequently, a rectangular fiber oriented horizontally along the longitudinal axis will experience normal stress conditions that are an average of the vertical and horizontal stresses. Similarly, square and circular fibers will experience normal stress conditions along the cross-sectional axis that are averages of the horizontal and vertical stresses.

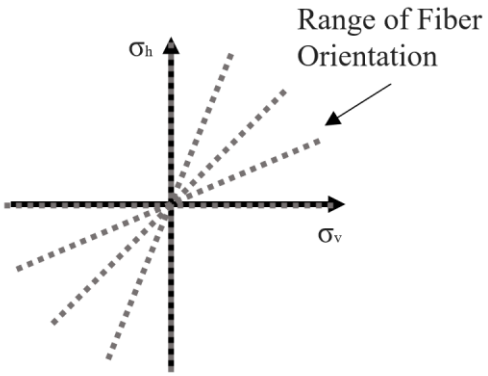

Figure 6: Range of possible fiber orientations (after Gregory 2006)

Gregory (2006) presented the following equation for the combined expression for the average stress conditions on an individual fiber, with respect to both the longitudinal and cross-sectional axes:

$$\sigma_{ave} = \sigma_v K_e$$

Equation 1

where:

$$K_e = 0.75\, K_e + 0.25 : \text{ the stress variable for fibers}$$

When the confining stress falls below a certain threshold, the fibers within the soil undergo slipping during deformation. However, once the confining stress exceeds a critical value, the fibers either yield or break. Considering practical factors such as fiber lengths, cross-sectional area, and ultimate tensile strength, it becomes evident that achieving the critical confining stress would necessitate an excessively tall embankment. Consequently, under nearly all practical conditions, the failure mechanism of FRS used for slope stabilization predominantly involves the pullout of fibers.

3.2 Effective Fiber Length

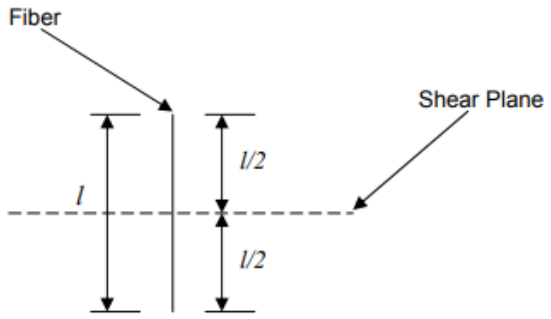

Figure 7: Effective fiber length (Gregory 2006)

Figure 7 illustrates that the effective length (L_e) of an individual fiber across a potential shear plane can range from zero to half of the fiber length. Consequently, the average effective length of a fiber becomes:

$$L_{e\ (ave)} = \frac{\frac{l}{2} + 0}{2} = \frac{l}{4}$$

Equation 2

where:

l: Length of fiber

3.3 FRS Shear Strength

Ranjan et al. (1996) and Maher and Gray (1990) introduced the following equations regarding the number of fibers intersecting a shear plane:

$$N_f = \frac{2V_r}{\pi d^2}$$

Equation 3

$$V_r = \frac{W_f}{G_s \gamma_w}$$

Equation 4

where:

N_f: Number of fibers intersecting the shear plane

d: Diameter of fiber, or equivalent diameter for noncircular fiber

V_r: Fiber volume ratio

W_f: Weight of fibers in a unit volume of FRS

G_s: Specific Gravity of fiber material

γ_w: Unit weight of water

Gregory (2006) derived an equation that describes the pullout resistance of any application rate of fibers caused by friction. Equation 5 expresses fibers' influence on the apparent frictional shear strength under stress conditions below the critical confining stress.

$$\tau_{frs\,\varphi} = L_e \pi d \sigma_v K_e f_\varphi N_f tan\varphi$$

Equation 5

where:

$\tau_{frs\,\varphi}$: Apparent increase in frictional shear strength due to fiber

f_φ: Interaction coefficient related to the frictional component of the shear strength

φ: Angle of shearing resistance of raw soil

Substituting the expressions for L_e and N_f into Equation 5, the equation can be reduced to (Gregory 2006):

$$\tau_{frs\,\varphi} = \frac{l}{2d} \sigma_v K_e f_\varphi V_r tan\varphi$$

Equation 6

Similarly, the equation for apparent increase in the cohesive shear strength due to fiber reinforcement would be (Gregory 2006):

$$\tau_{frsc} = \frac{l}{2d} f_c V_r c$$

Equation 7

where:

τ_{frsc} : Apparent increase in cohesive shear strength due to fiber when $\Delta\varphi_{frs} = 0$

f_c : Interaction coefficient related to the cohesive component of the shear strength

c : Cohesion of raw soil

Equation 7 assumes there that the change in friction angle will be zero, but this is not the case. Consequently, Equation 7 presents an uncorrected cohesion increase. Gregory (2006) suggested that this correction is related to the difference in slope of the two strength envelopes projected back to the axis from the point of "rotation" of the FRS strength envelope (Figure 8).

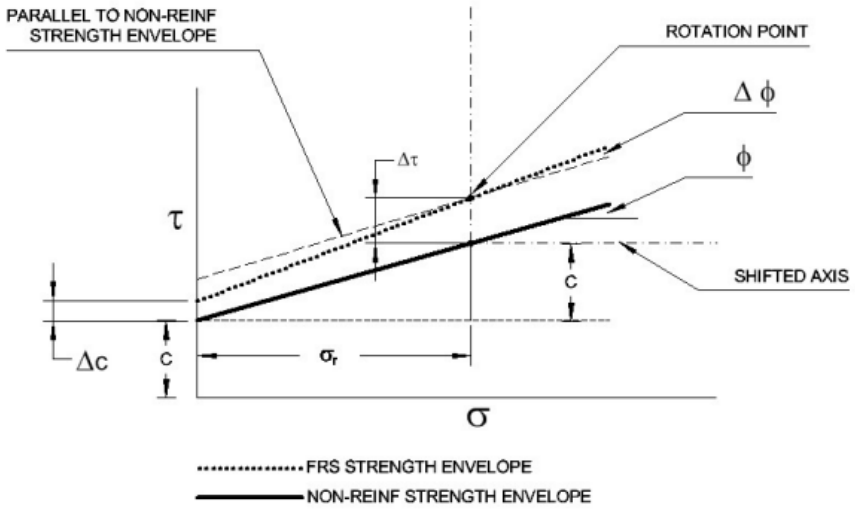

Figure 8: Rotation point of FRS strength envelope (Gregory 2006)

And therefore, he proposed the following equations to implement the corresponding correction:

$$\sigma_r = \frac{c}{tan\varphi}$$

Equation 8

$$\Delta c_{frs} = \tau_{frsc} - \sigma_r(tan\varphi_{frs} - tan\varphi)$$

Equation 9

$$c_{frs} = c + \Delta c_{frs}$$

Equation 10

where:

σ_r : Normal stress value at which the cohesion correction factor is calculated

$tan\varphi$: Tangent of the non-reinforced φ value

c : Non-reinforced cohesion value

3.4 Pullout Resistance and Interface Shear Strength

Pullout resistance of a reinforcement element, P_r, and interface shear strength of soil and reinforcement (τ_{iss}) are determined using Equations 11 and 12, respectively (Berg et al. 2009, Esmaili, 2014):

$$P_r = F^* \alpha \sigma_v' L_e C$$

Equation 11

$$\tau_{iss} = c_a + (\sigma_n - u_a)\, tan\delta'$$

Equation 12

where:

$F^* = \tan \delta_{peak}$: Pullout resistance factor

δ_{peak}: Equivalent peak friction angle of the soil-geosynthetic interface (°)

α: A scale effect correction factor to account for a nonlinear stress reduction over the embedded length of highly extensible reinforcement

σ_v': Effective vertical stress at the soil-reinforcement interface

C: Reinforcement effective unit perimeter; e.g., C = 2 for strips, grids, and sheets

σ_n: Normal stress on the interface

c_a: Interface adhesion at specific suction

u_a: Pore air pressure

δ': The angle of friction between soil and reinforcement with respect to $(\sigma_n - u_a)$

As indicated by Berg et al. (2009) and Esmaili (2014), pullout tests are commonly used to determine the parameters α and F^* for different types of reinforcement materials. The correction factor α is influenced by the extensibility and length of the reinforcement, and, its recommended value is 0.6 (Berg et al., 2009). The parameter F^*, particularly in reinforcement types like geogrids and welded wire mesh, encompasses both passive and frictional resistance components (Palmeira, 2004; Abu-Farsakh et al., 2005; Berg et al., 2009).

Chapter 4 – Materials and Methods

A series of laboratory tests and analysis was carried out as described in this and the following chapters to achieve the objectives of the study as outlined in Chapter 1.

4.1 Fiber Materials

The facemasks used for the fabrication of fibers were produced by the company *FFG Personal Protection Equipment* and purchased in boxes of 50 units (Figure 9).

Figure 9: Information on commercial facemasks used in the study

4.1.1 Selection of Facemask Layer to Fabricate FRS Fibers

The tensile strength of the fibers was determined in general conformance with the ASTM D4632 test protocol. Consequently, the tests were carried out on 25.4 mm x 152.4 mm x 0.0127 mm strips for each of the different layers of the mask, with a loading rate of 305 mm/min, securing 25.4 mm of the specimen on each clamp with a starting distance

between clamps of 101.6 mm. Figure 10 illustrates the methodology of cutting the facemask layers into strips for tensile testing, using a precision knife and a ruler.

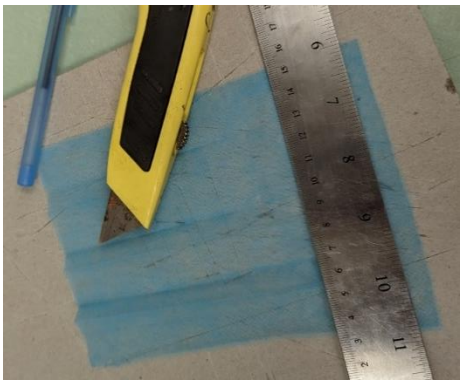

Figure 10: Precision knife and ruler used for cutting facemasks into strips for tensile strength testing

Figure 11 shows the DSTM Universal Testing Machine, a 10 kN (2,250 lb.) tensile testing machine used in this study to determine the strength of face mask materials.

Figure 11: The Universal Testing Machine used in this study

4.1.2 Estimation of Soil-Fiber Interface Shear Strength

Similar to the procedures outlined in Esmaili's study (2014), the soil was first moistened to achieve the desired optimum moisture content. A piece of reinforcement material, of square dimensions of 60 x 60 mm, was attached to a piece of wood using commercial superglue. The lower half was filled with metallic plates and then the piece of wood with the fiber material facing up, such that it was positioned by half of the test cell in contact with the soil. The upper and lower halves of the cell were securely fastened together using bolts. Next, the wet soil was compacted in four layers, each measuring 3mm in thickness, on the upper half of the test cell. The test was conducted on strips made from the inner layer of a facemask and black geotextile material, using overburden pressures of 50, 100 and 150 kPa, and a shear loading rate of 1 mm/min as indicated in ASTM D5321. Figures 12, 13 and 14 provide a visual depiction of the setup used in this test.

Figure 12: Facemask glued to piece of wood. Lower half of test cell

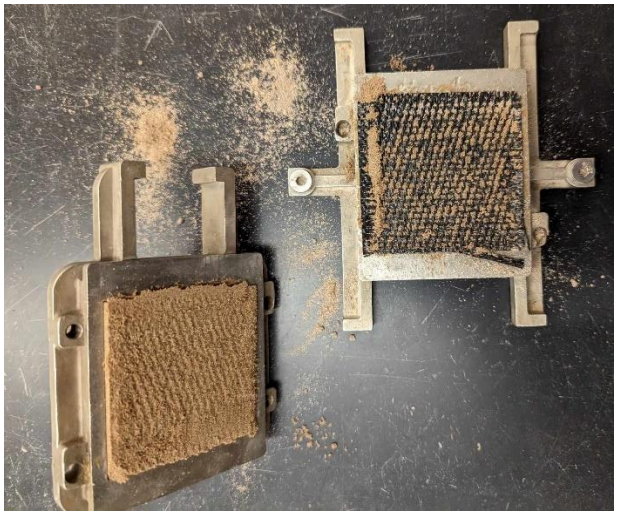

Figure 13: Interface shear test load cell with geotextile after test

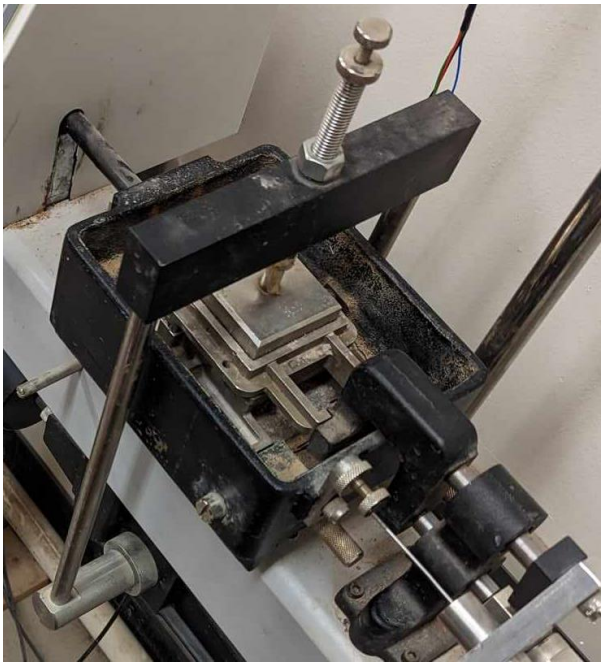

Figure 14: Test cell on the interface shear test machine

Figure 15 shows the ELE International Direct/Residual Shear Test Set used in this study to determine pullout strength of fiber materials.

Figure 15: Direct/Residual Shear Test Set used in the study

4.1.3 Fabrication of Fibers

For the triaxial test of FRS, the facemasks were cut by hand and stored in plastic bags until the time of specimen preparation. Multiple fabrication methods were tested for the creation of strips to be used in FRS specimens. First, cutting the masks by hand was found to be imprecise and inefficient for producing sufficient fibers for the project. An alternative approach was attempted using laser cutters available in the OU Innovation Hub (https://www.ou.edu/innovationhub), but it was found to be unsuitable due to the high temperatures resulting from the cutter, which melted the material, and even caused it to burn. Ultimately, the most suitable solution found was to use a cutting mold and a precision knife as shown in Figure 16. The cutting mould was made of wood using the laser cutting machine. The strip cutting process involved flattening facemasks for one day by placing them between plastic boards with weights on top, and then using a precision

knife and the laser-cut mould to cut strips from the flattened masks. Strips are shown in Figure 17.

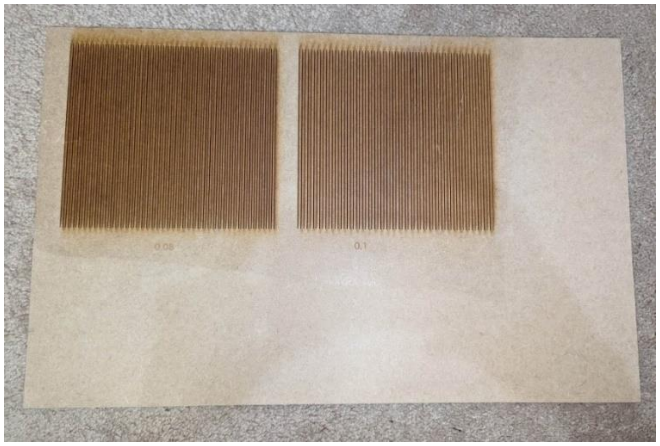

Figure 16: Laser-cut mold used to produce thin strips from the facemasks

Figure 17: From top to bottom, facemask fibers of 2.5 x 51 mm, 5.1 x 51 mm and geotextile fibers of 2.5 x 51 mm

The fibers used were produced using the inner polypropylene layer of the facemasks, which was determined to be the strongest layer from the tensile strength tests conducted on all facemask layers.

4.2 Soil Materials

A blend of soil was produced following a series of preliminary tests for the triaxial tests in this study. The objective was to produce a generic type of soil that contained a considerable quantity of fines and yet, it was sufficiently permeable to help expedite the testing program, which involved a significant number of triaxial tests. The final blend was a soil that included 80% sand passing sieve No. 40, and 20% limestone, classified as Poorly Graded Sand (SP) according to the Unified Soil Classification System (USCS). A brief description of the preliminary tests to finalize the soil blend is provided in the following section.

4.2.1 Preliminary Tests on Soil Materials

One main factor in finalizing a blend of soil for the study was to keep the time requirements for each triaxial test within a reasonable time period. This was done given that this study involved a comparison of the shear strength properties of FRS specimens with those of the comparable raw soil in general terms, as opposed to investigating an FRS solution for a particular site or soil type. Therefore, the time requirements for different stages of triaxial tests on several candidate soils were determined through a series of preliminary triaxial tests. Single stage triaxial tests were carried out on raw clay and sand specimens after determining their OMC values using proctor tests. These tests allowed for the saturation and consolidation times for each soil to be determined, which are reported in Table 3.

Table 3: Summary of preliminary triaxial tests on different soil types to select a suitable soil for the study

Specimen Type	Test Start Date	Total Duration (hours:min)	Saturation (hours:min)	Consolidation (hours:min)	Comments
Clay	12/22/2022	137:08	47:26	89:42	Average total duration of 150 hours
Clay	01/02/2023	162:54	51:52	111:03	
13% Limestone 87% Sand	02/13/2023	0:0	-	-	Impossible to stabilize specimen in triaxial chamber. Discarded as soil candidate
30% Limestone 70% Sand	02/16/2023	206:48	89:53	116:55	-
20% Limestone 80% Sand	02/25/2023	123:29	26:10	97:20	Average total duration of 89.3 hours
20% Limestone 80% Sand	03/03/2023	55:02	29:42	25:21	

The conclusion of this evaluation process was that an 80% sand, 20% limestone blend was best suited for this study due to its comparatively lower saturation and consolidation time requirements, in addition to its sufficient stability when set up in the triaxial test cell. Figure 18 shows specimens after conducting triaxial testing, and Figure 19 shows example images of different types of soil tested in this preliminary phase of the study.

Figure 18: Preliminary test specimens after triaxial testing

Figure 19: Clay, 30% Limestone Sand, and 20% Limestone Sand specimens after triaxial tests

Preliminary triaxial testing with this sand showed that the saturation stage of the triaxial tests could be completed within 24 hours, making it a time-efficient soil that could be tested sufficiently within the period available for the study.

4.2.2 Sources of Ingredient Soils

The sand used for the triaxial test specimens was obtained from a site on the west side of the outdoor test station at the OU Fears Structural Laboratory on south campus (Figure 20). Two types of limestone were procured from Dolese Bros. Co. to mix with the sand for testing (Figure 21). The first type, labeled "Ag. Lime", consisted of a material with little processing and therefore, higher sample to sample variability in particle size. Consequently, this lower-quality material could exhibit inconsistencies in its characteristics. In contrast, the second type of limestone, labeled "Industrial Materials", had undergone more thorough processing by the manufacturer, resulting in less variation in the soil composition across different samples. Therefore, the latter type of limestone was used to prepare the triaxial specimens in order to increase their uniformity and reliability, and help obtain more accurate test results.

Figure 20: Source of the sand used in the study at the Fears Structural Laboratory (shown with a red circle). Image from Google Maps

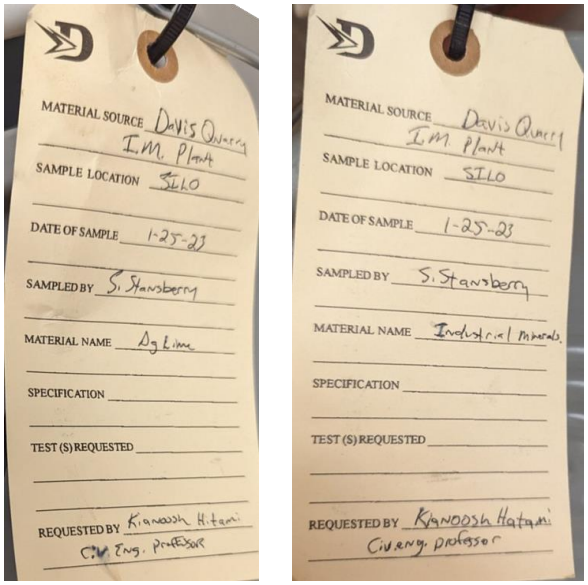

Figure 21: Information on limestone buckets as delivered by Dolese Bros. Co.

4.2.3 Preparation of Soil Specimens

The sand was manually collected using a shovel and placed into buckets that were then transported to the laboratories in the Carson Engineering Center (CEC). Upon arrival at the laboratory, the soil was evenly spread out on trays and any large rocks or organic matter were manually removed from the soil. Soil samples were afterwards placed in ovens to dry for 24 hours at 212 °F (100 °C) following ASTM D2216. Afterwards, the sand was sieved for 10 minutes following the recommendation in ASTM C136. The objective was to collect the particles passing through sieve No. 40 but retained on sieve No. 200. This specific size fraction was found suitable for the type of soil that was desired for triaxial testing as discussed in Section 4.2.1. The W.S. Tyler® RX-20 Rotary Sifter shown in Figure 22 was used to sieve the sand used in this study.

Figure 22: Rotary Sifter used to process the soil in this study

The manual mixing process of soils involved placing the sand and limestone in a weighed bucket at the ratio of 80% sand and 20% limestone, as discussed in Section 4.2.1. The bucket was filled to approximately one third of its total capacity to allow ample space for the soil to move around in the bucket during the mixing procedure. To prevent any unintended loss of materials, the bucket was sealed with a tight lid, and it was firmly held and rotated in multiple directions to ensure that the sand and limestone were thoroughly mixed. Mixing by hand was also conducted and the procedure was concluded using visual inspection when a homogeneous and consistent soil mixture was observed.

4.2.4 Soil Classification Tests

Standard soil classification tests were carried out on the soil to determine its gradation and Atterberg limits (i.e. Liquid Limit, Plastic Limit and Plasticity Index) using the

corresponding test standards, which included one-point method in ASTM D4318 and ASTM D6913, respectively.

4.2.5 Standard Proctor Tests

Proctor tests were carried out in accordance with ASTM D698, Method A. A total of 5 specimens were tested in order to establish a moisture-density relationship curve and identify the gravimetric optimum moisture content (OMC) and maximum dry density of the soil. This information was used to prepare the raw soil and FRS specimens for triaxial testing in the next stage of the study.

4.3 Testing of Fiber Reinforced Soil Specimens

Similar to the case of raw soil, preparation of triaxial test specimens involving soil and facemask fibers was also carried out following the methodology described by Gregory (2006). The soil was spread evenly on a flat surface. Afterwards, a carefully weighed quantity of strips was spread on the top of the soil and was mixed manually to obtain a visually uniform blend, as shown in Figure 23. The mixture of soil and strips was placed and compacted carefully in the triaxial mold using the same procedure described in Section 4.2.3 and in this way prepare FRS specimens for triaxial testing.

Figure 23: Manual mix of soil and fiber strips

Taking the corresponding minimum and maximum stresses for each stage of the triaxial tests, three Mohr's circles were plotted on a shear vs normal stress graph. The best fit line for the maximum shear value of each circle was used to plot the K_f line (p vs q failure envelope). This subsequently allowed the estimation of parameters α, m, effective friction angle (ϕ'), and effective cohesion (c'), using the following relations:

$$\varphi' = sin^{-1}(tan(\alpha)) \qquad \textit{Eq 13}$$

$$c' = \frac{m}{cos\,\varphi'} \qquad \textit{Eq 14}$$

Figure 24 shows a schematic representation of the above parameters.

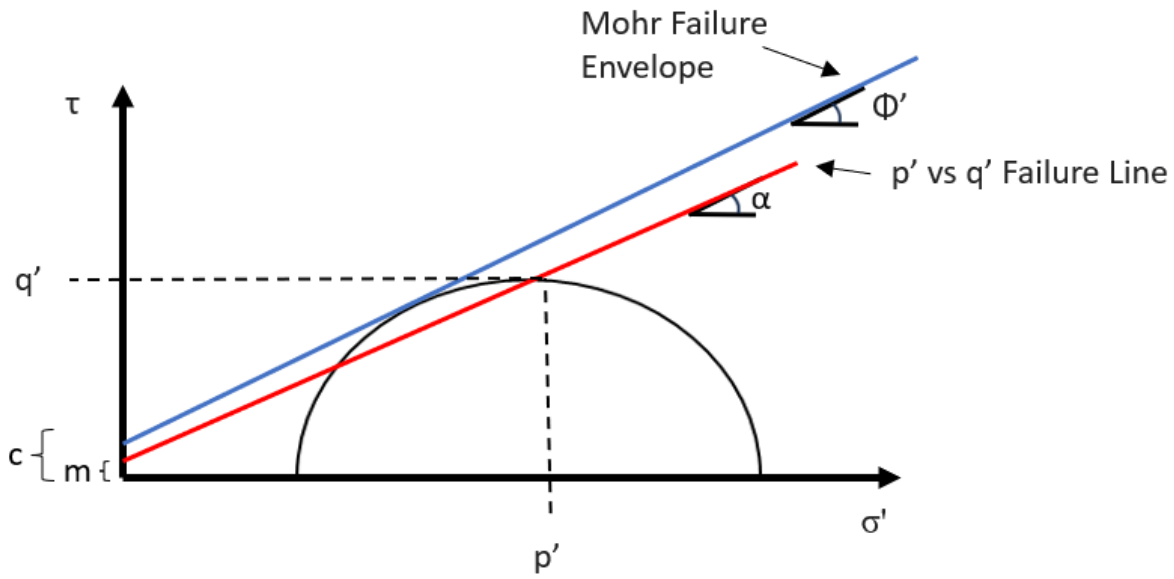

Figure 24: Mohr Failure envelope and p' vs q' failure line (K_f line)

4.3.1 CUIC Triaxial Tests

The studies surveyed in Chapter 2 indicate that triaxial testing of soil specimens is a common method to examine the effects of fiber reinforcement on their mechanical behavior. Therefore, the strength and mechanical performance of the raw soil and FRS specimens were measured through a series of CUIC tests in this study in accordance with ASTM D4767 test protocol.

Figure 25 shows the equipment and a typical setup for triaxial tests that were carried out in this study. The GDS Triaxial Automated System (GDSTAS) featured a confining cell with a maximum capacity of 3.5 MPa, and complementary software which allowed for multistage triaxial testing. The GEOTAC TruePath Automated Stress Path System (TASPS) featured a confining cell with a maximum capacity of 2 MPa, and complementary software which only allowed for single stage triaxial testing. This issue

was overcome by running the software normally for the first stage, closing the confining cell valves to maintain the pressures, and then reopening them again after having restarted the software for a new test where the saturation stage was skipped.

Figure 25: GDSTAS in CEC B7 (left) and TASPS in CEC B4 (right)

Figure 26 illustrates triaxial apparatus setup. Specimens were then placed inside the triaxial chamber and were set up to carry out the different stages of the triaxial tests. In the first phase, the specimens were saturated until the B-value as measured and as shown on the computer display reached or exceeded 0.95. Afterwards, the specimens were consolidated and subsequently sheared using a multistage approach. Consolidation of the specimen was deemed completed when the back volume - the volume of water within the specimen - became constant. The shearing of specimen was deemed completed when the specimen reached 5% axial strain, based on the work by Nambiar et al. (1985) and Soranzo (1988) as discussed in Chapter 2. Considering that the main application of

reinforced soil was for repair of shallow slope failures, effective confining pressures applied on the specimens were kept to a maximum value of 100 kPa. This value is still significantly greater than the actual confining stresses expected in shallow failure of roadway embankments (e.g. 30-50 kPa). However, this higher value was found to be necessary to help to complete different stages of the triaxial tests in a reasonable amount of time.

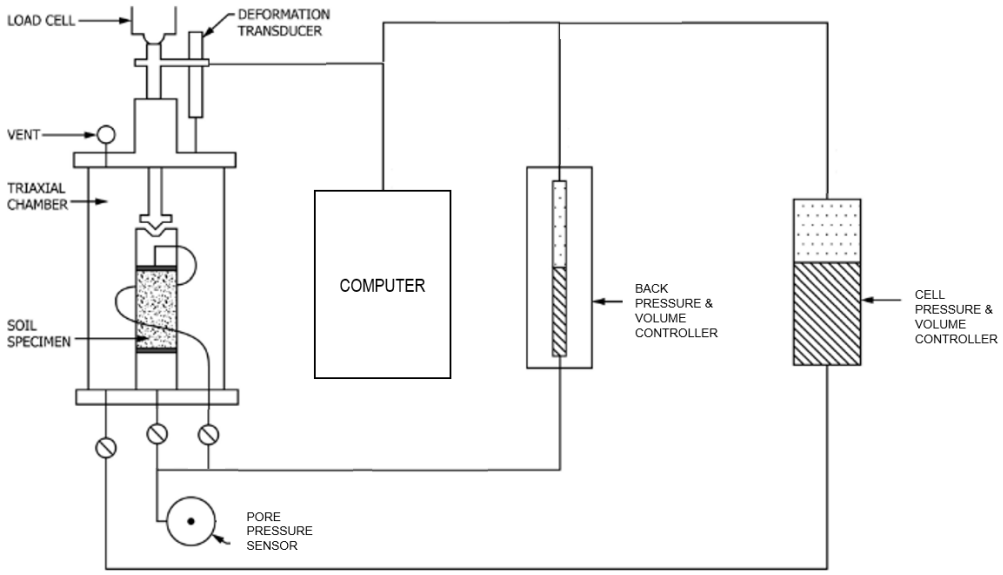

Figure 26: Schematic of triaxial apparatus (ASTM D4767)

Results of the triaxial tests were used to calculate the cohesion and friction angles of different soil specimens, using the Mohr-Coulomb failure criterion, and the stress-strain relationship in order to evaluate any improvements in strength in FRS specimens relative to that of the raw soil. Table 4 indicates the number of specimens and variables that were examined in the triaxial tests carried out in this study.

Table 4: Variations in FRS specimens relative to the fibers' attributes

Specimen Type	No. of Specimens	Fiber Concentration (kg/m^3)	Fiber Dimensions (mm)
Facemask	2	0	N/A
	1	0.8	0.25 x 51
	1	1.2	
	1	1.6	
	1	0.8	0.50 x 51
	1	1.2	
Geotextile	1	0.8	0.25 x 51
	1	1.2	

4.3.2 FRS Specimen Preparation

Soil specimens of 71 mm diameter and 142 mm height were prepared at their optimum moisture content in a steel mold, following the procedure recommended by Gregory (2006). First the soil was spread on a flat tray, with fibers evenly spread on top, and then water was added to the soil while mixing these components. The soil, or the FRS as applicable, was then placed in the mold in three lifts, each of which was compacted with 10 blows of a standard proctor hammer to maintain consistent compaction between specimens. Pouring of the FRS mixture into the mold was done from varying angles to maximize the spreading of the fibers in the specimen and prevent their accumulation towards one side of the specimen. In the first two lifts, grooves were made on the top surface before adding the subsequent layer to facilitate intermixing of the soil across the lifts and minimize a stratified configuration within each specimen.

4.3.3 Visual Inspection of FRS Specimens

FRS specimens were visually examined before and after each triaxial test to evaluate the suitability of their preparation method in general, and specifically relative to fiber distribution. This evaluation aimed to ensure that the distribution of fibers within the specimen was even and that their orientation was random. Figure 27 shows a dissected specimen that broke before triaxial testing and was studied before being discarded. It also shows specimens dissected horizontally after triaxial testing for examination.

(a) (b)

Figure 27: Dissected FRS specimens (a) FM-D50-C0.8 (discarded, not tested), (b) FM-C25-C0.8 and FM-C25-C1.2 after triaxial tests

4.3.4 Labeling of Triaxial Test Specimens

In order to facilitate the identification of different triaxial test cases, they were labeled using an alphanumeric system as shown in Table 5. The labels incorporate key variables relative to the soil type, fiber dimensions and concentration. For instance, the first FRS specimen tested with fibers that were made of facemask, with dimensions of 5.1 mm × 51 mm, and a concentration of 0.08 kg/m^3 is labeled as FM-D50-C0.8 per Table 5.

Table 5: Labels used to identify different triaxial test cases

Fiber Material		Fiber Dimensions (mm)		Fiber Concentration (kg/m^3)	
Facemask	FM	2.5 × 51	D25	0.8 kg/m^3	C0.8
Geotextile	GT	5.1 × 51	D50	1.2 kg/m^3	C1.2
				1.6 kg/m^3	C1.6

4.4 Summary

Table 6 summarizes the matrix of tests that were carried out in this study, and Table 7 provides additional information on the Multistage CUIC Triaxial Tests.

Table 6: Summary information on the triaxial tests carried out in this study

Test	Standard Followed	No. of Specimens	Variables	Parameters of Interest	Constants
Tensile Testing of Facemasks	ASTM D4632	16	Fiber Material	σ_{1f}, ε	l/w, $\dot{e}$
Soil Atterberg Limits	ASTM D4318	6	ω	PL, LL	Soil type
Interface Shear Test	ASTM D5321	21	Fiber Material, σ_3	f_ϕ	Soil type, $\dot{e}$
Standard Proctor Test	ASTM D698	20	ω, ρ	OMC, $(\gamma_d)_{max}$	Compaction effort, Soil type
Multistage CUIC Triaxial Tests	ASTM D4767	12	ρ	ε, c, ϕ	Soil type, OMC, σ_3, $\dot{e}$

where,

c Cohesion intercept of the soil

$\dot{e}$ Shearing rate

l/w Fiber aspect ratio

LL Liquid Limit

PL Plastic Limit

ε Axial strain in soil specimen

f_ϕ Soil-fiber interaction coefficient

ϕ Internal friction angle of the soil

σ_{1f} Failure axial stress

σ_3 Confining Pressure

ω Gravimetric water content

ρ Fiber concentration

$(\gamma_d)_{max}$ Maximum dry weight of soil

Table 7: Different stages in multistage CUIC triaxial testing of soil and FRS specimens

Stage	No. of Steps Involved	Cell Pressure (kPa)	Back Pressure (kPa)	Strain Rate (%/min)	Indicator of Completion	Purpose
Saturation	1	770	750	N/A	B-value >= 0.95	Fill specimen's voids with water
Consolidation	3	800, 1000, 1200	750		Back volume becomes constant	Dissipation of excess pore water pressure within the soil specimen
Shearing	3			0.35[1]	5% Strain	Determine the shear strength parameters of the soil, including its cohesion and internal friction angle

[1] Jafarian et al. (2013), Derkaoui et al. (2016) and Saeidaskari (2021)

Chapter 5 – Laboratory Results of Test on Fiber and Soil Materials

5.1 Tensile Strength Tests

Twelve masks were separated to its three layers and cut into 25.4 mm (L) x 0.0127 mm (W) x 152.4 mm(H) strips and loaded onto the tensile testing equipment, as shown in Figure 28. The rate used was 305 mm/min.

Figure 28: From left to right, facemasks strip loaded on the machine before, during and after tensile testing

5.1.1 Inner Layer

From handling the inner layer of the facemasks and pulling it apart by hand, it was observed that this was likely to be the strongest layer of material in relation to the other two layers. Twelve strips of this material were loaded onto the tensile testing equipment and tested. The results can be observed in Figure 29.

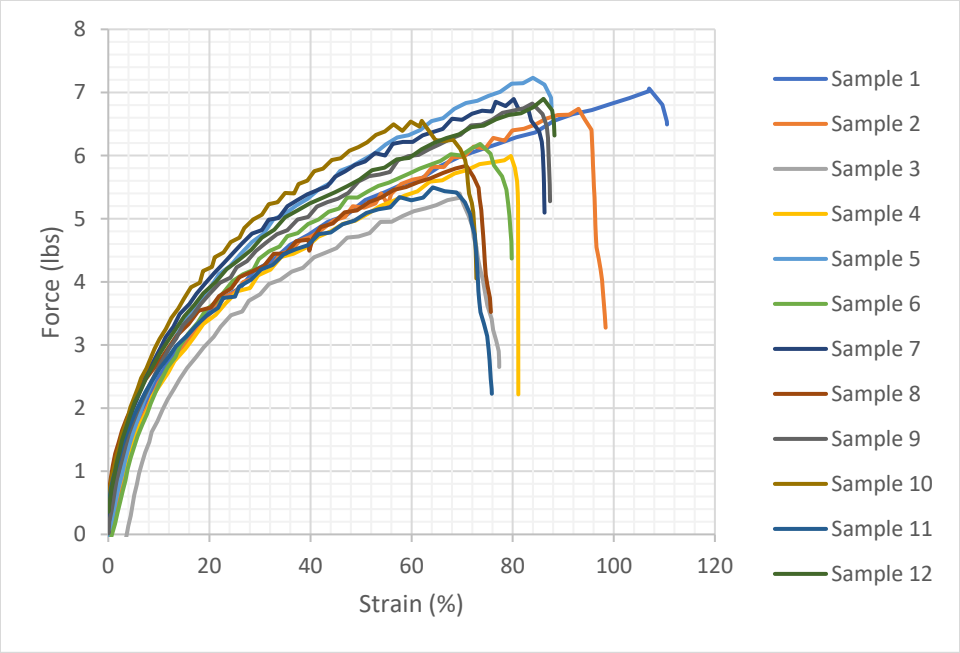

Figure 29: Tensile Test Results - Inner Layer

Maximum force values observed for each sample are presented in Table 8.

Table 8: Tensile Test Results for the Inner Layer

Strip	Max Force		Strain (%)
	(lbs)	(N)	
1	7.06	31.40	106.97
2	6.74	29.98	93.01
3	5.4	24.02	69.48
4	5.99	26.64	79.64
5	7.23	32.16	84.02
6	6.18	27.49	73.57
7	6.9	30.69	80.19
8	5.84	25.98	70.85
9	6.82	30.34	83.89
10	6.55	29.14	73.63
11	5.5	24.47	64.19
12	6.9	30.69	86.1
Average	6.43	28.58	80.46

The average force that this sample was capable of sustaining was 28.58 N. Compared to other evaluated layers, this is conclusively the strongest layer of material present in the FFG facemasks.

5.1.2 Outer Layer

The characteristically blue outer layer of the facemasks was tested. Figure 30 illustrates the results for the testing of four strips. No further testing was conducted after the first four specimens indicated that this layer was weaker than the inner layer.

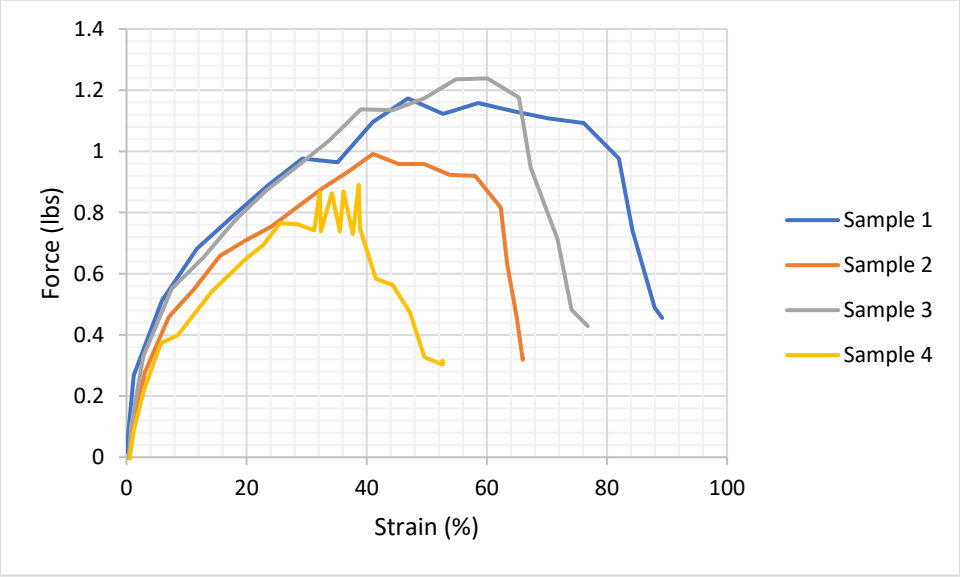

Figure 30: Tensile Test Results - Outer Layer

Table 9 presents the important values obtained from this test. The average force that the material was capable of sustaining was 4.76 N, which is lower than what was observe for other layers.

Table 9: Tensile Test Results for the Outer Layer

Strip	Max Force		Strain (%)
	(lbs)	(N)	
1	1.17	5.20	59.47
2	0.99	4.40	44.02
3	1.24	5.52	51.20
4	0.89	3.96	35.13
Average	1.07	4.76	47.46

5.1.3 Filter Layer

In the process of separating the masks into layers, the filter layer, made from white melt-blown polypropylene, demonstrated to have very poor tensile strength properties overall. The layer easily ruptured with simple handling of the material while producing the strips. Also, when loading of the strips made from this material on the equipment, they ruptured when applying minimal tension on them while placing them in the clamps. From these observations, it was concluded that this paper material was unsuitable for the purposes of this study, and tensile testing procedures were not conducted on strips made from this layer.

5.2 Soil-Fabric Interface Shear Tests

Figures 31 and 32 show interface shear test results for the soil and two fabrics, the HP570 geotextile in the machine direction and the facemask, for comparison purposes.

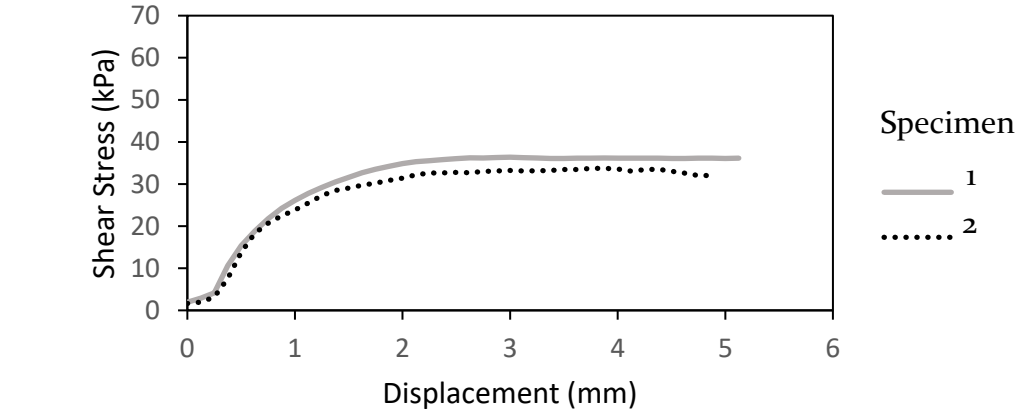

(a)

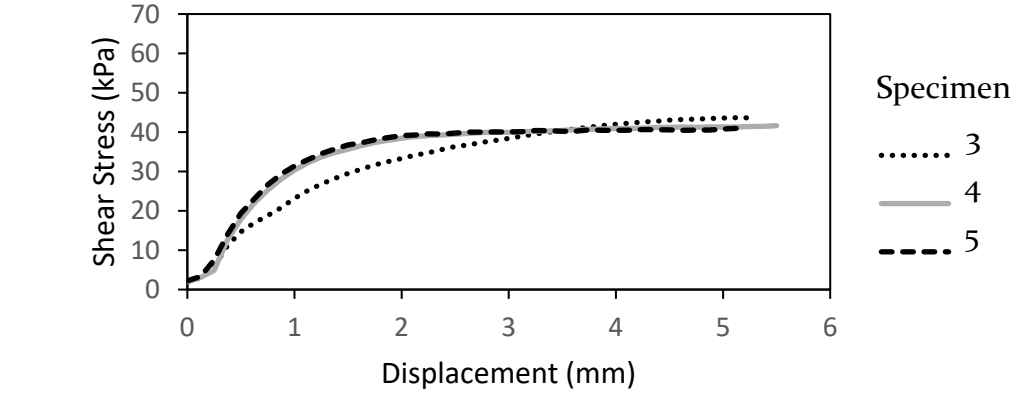

(b)

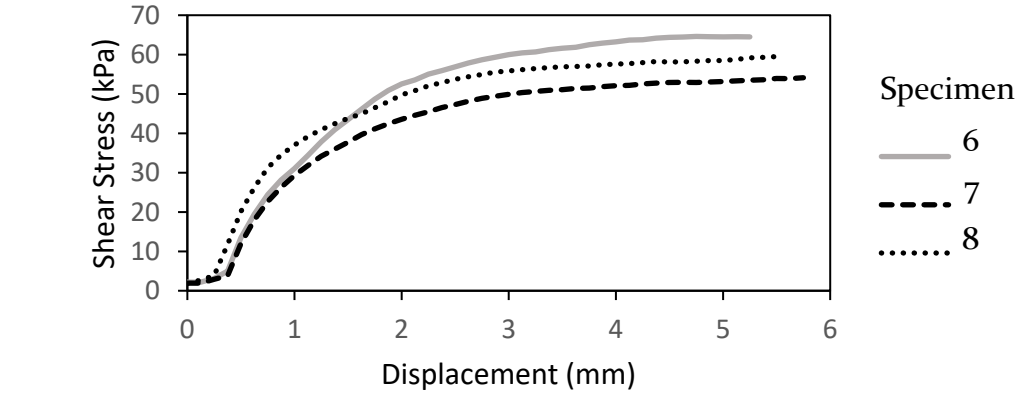

(c)

Figure 31: Results for the soil-geotextile interface shear tests at (a) 50 kPa, (b) 100 kPa, and (c) 150 kPa overburden pressure

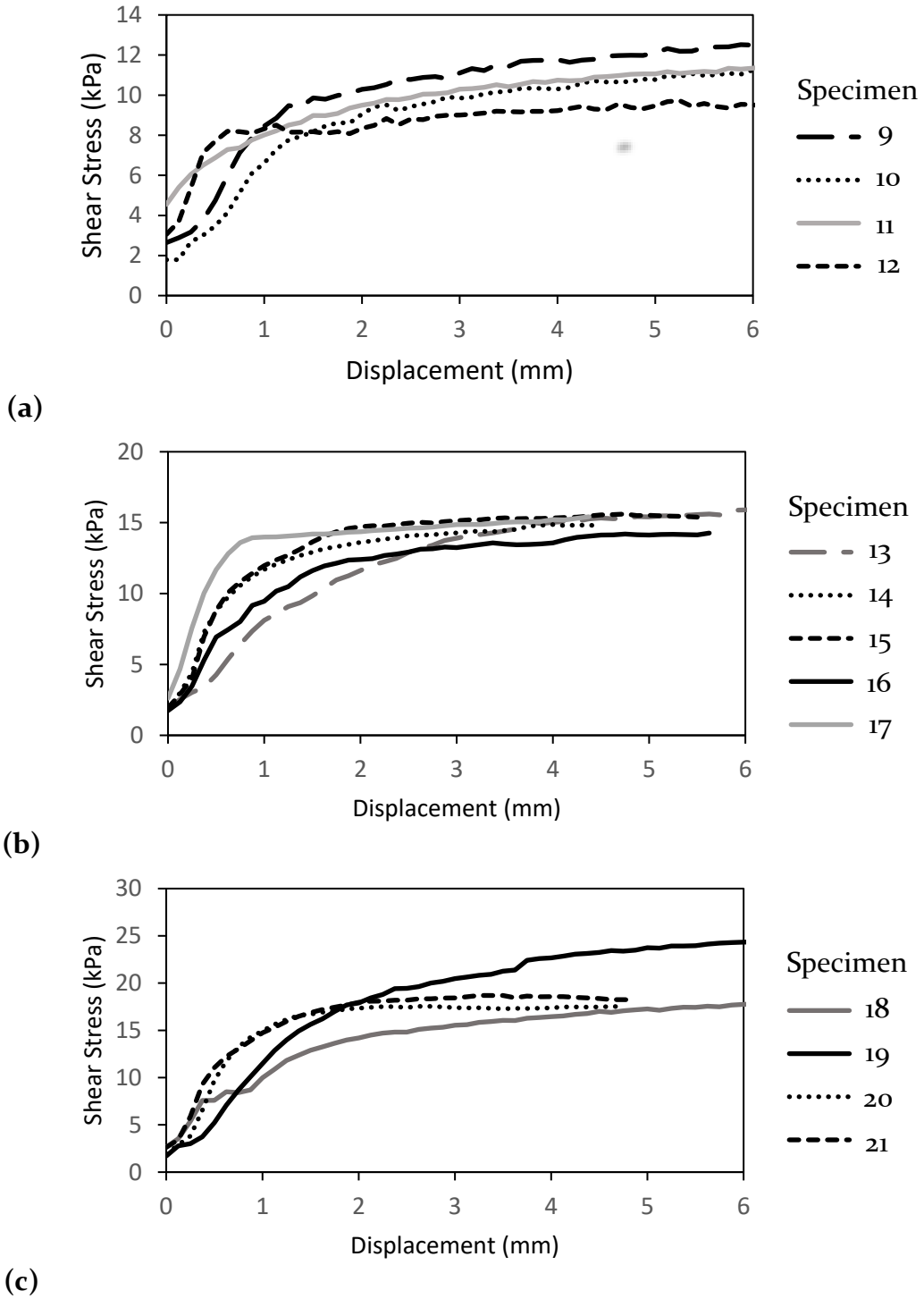

Figure 32: Results for the soil-facemask interface shear tests at (a) 50 kPa, (b) 100 kPa, and (c) 150 kPa overburden pressure

Taking the average maximum shear stress from each case, Figure 33 presents the overall results from the interface shear test conducted on the facemasks and geotextile specimens.

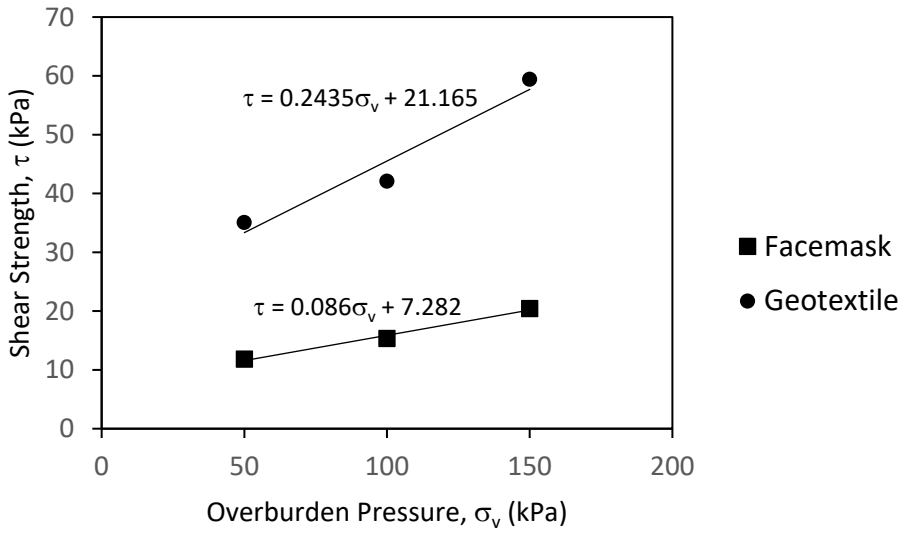

Figure 33: Soil-fabric interface shear test results

The y-intercepts of the lines depicted in Figure 33 represent initial estimates of soil cohesion values, while the slope of each line serves as an approximation of the friction angle between the soil and the reinforcement materials. Notably, it is evident that the facemask polypropylene exhibited lower values for both parameters when compared to the geotextile used as a reference. However, it's important to note that the woven pattern of the geotextile leads to a stronger frictional interaction with soil when compared to individual fibers used in FRS applications. Therefore, the shear strength properties for the geotextile specimens in Figure 33 are considered as upper-bound values for the

corresponding fibers if used in FRS applications. Nevertheless, the interface shear test results help estimate ballpark interface shear strength values for FRS applications for both materials examined.

5.3 Differences in Unit Mass of Fiber Materials

Preparation of triaxial FRS specimens with geotextile and facemasks fibers made it evident that the unit weights of each material were significantly different, as very different quantities of each material were needed to reach a given fiber concentration on a specimen. A high precision scale was used to measure the mass of individual fibers of each material, as shown in Figure 34.

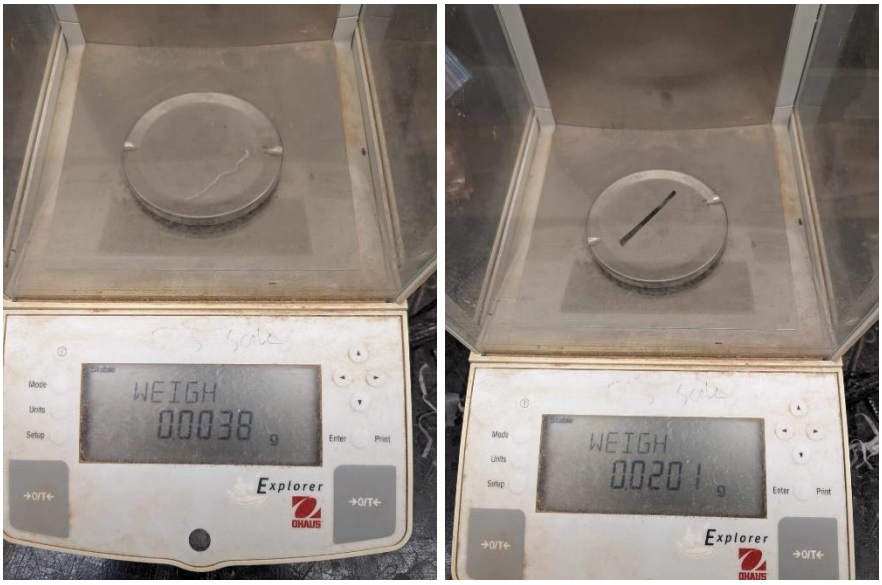

Figure 34: High precision scale with facemask (left) and geotextile (right) fibers

Table 10 presents the results of measurements of the mass of 2.5 mm × 51 mm individual fibers using a high precision scale. The data in the table illustrates that the mass of

geotextile 2.5 × 51 mm fibers can be roughly 15 times greater than that of facemask fibers. This significant difference in mass certainly affects the amount of material needed to achieve a specific concentration on an FRS specimen. Thus, the extent of soil-fiber interaction due to different total area of soil-fiber contact can be expected to play a role in the performance of FRS specimens.

Table 10: Measured mass of individual 2.5 mm × 51 mm fibers (in grams)

Sample	Geotextile	Facemask	Sample	Geotextile	Facemask
1	0.0211	0.0035	7	0.0200	0.0035
2	0.0206	0.0032	8	0.0205	0.0038
3	0.0201	0.0036	9	0.0210	0.0030
4	0.0208	0.0032	10	0.0209	0.0028
5	0.0211	0.0040	11	0.0215	0.0024
6	0.0201	0.0030	12	0.0216	0.0029
Average Geotextile Fiber Unit Mass			Average Facemask Fiber Unit Mass		
0.0208 grams			0.0032 grams		

5.4 Soil Classification Test

Figure 35 shows the particle distribution curve of the sand.

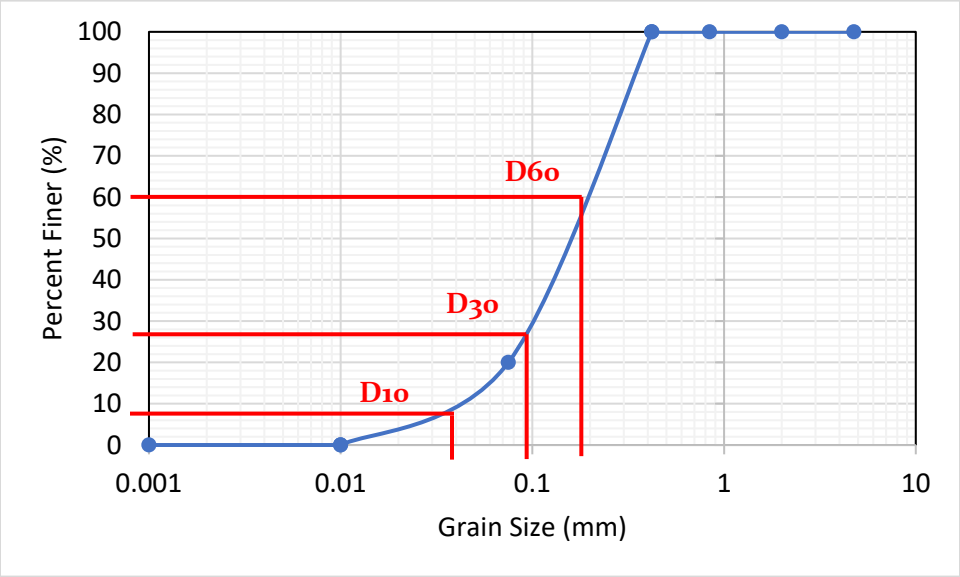

Figure 35: Particle size distribution of the sand

Table 11 shows the corresponding coefficients of uniformity and of curvature, as well as soil classification.

Table 11: Specific Gravity, Coefficient of Uniformity, Coefficient of Curvature, and USCS Soil Classification

Specific Gravity	Coefficient of Uniformity (C_u)	Coefficient of Curvature (C_c)	USCS Classification
2.42	5	1.25	SP

Lastly, all soil mixtures, with and without fiber reinforcement elements, were found to be non-plastic in the Atterberg Limits tests.

5.5 Standard Proctor Test

Figure 36 shows the standard proctor test results for soil compaction.

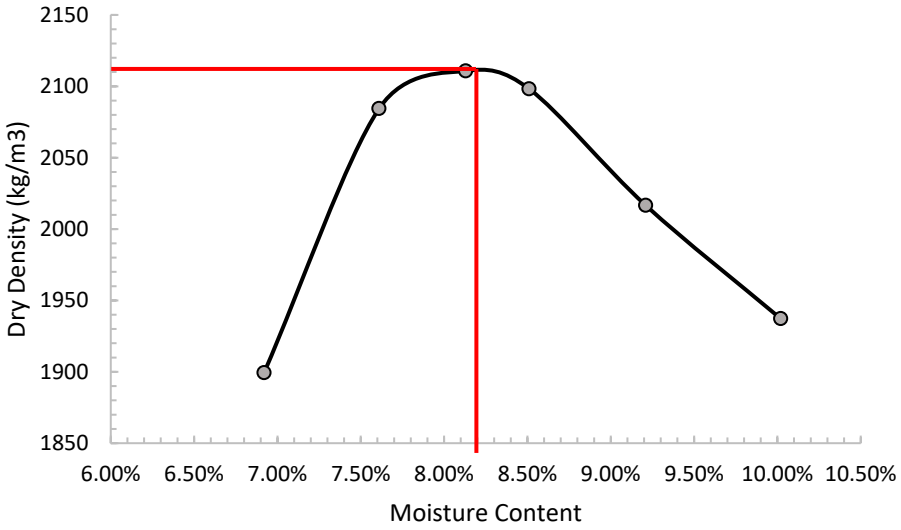

Figure 36: Standard Proctor Test Results for Soil Compaction

Table 12 shows the corresponding optimum moisture content and maximum dry density.

Table 12: Parameters from Standard Proctor Test Results for Soil Compaction

Maximum Dry Density	Optimum Moisture Content
2210 kg/m³	8.2 %

5.6 Summary

Table 13 summarizes the results obtained from different tests conducted on fiber materials.

Table 13: Summary of fiber material properties

[1]

Parameter	Facemask (Inner layer)	Geotextile
Ultimate Tensile Strength[1] (N)	28.6	178[2]
Soil-Fabric Interface Friction angle[3] (°), δ	5.0	14.0
Fiber Mass (grams)[4]	0.0032	0.0208
Specific Gravity G_s[5]	0.90–0.96	0.90–0.96

Determined for a 25 mm-wide fiber

[2] From manufacturer's technical datasheet (Appendix C)

[3] From Figure 33

[4] 2.5 × 51 mm specimen size

[5] Koerner (2005)

Table 14 summarizes the results obtained from different tests conducted on soil materials.

Table 14: Summary of soil material properties

Parameter	Soil Material
USCS Classification	SP
Specific Gravity	2.42
Coefficient of Uniformity (Cu)	5
Coefficient of Curvature (Cc)	1.25
Maximum Dry Density	2210 kg/m3
Optimum Moisture Content	8.2 %

Chapter 6 – Laboratory Results of CUIC Triaxial Tests

In this chapter, the focus is solely on displaying the results derived from laboratory tests. For related discussions, refer to Chapter 7, where corresponding analysis and interpretations are provided.

6.1 Triaxial Testing

Figure 38 show consolidation curves for FRS specimens set up and tested as described in Section 4.2.6. Consolidation was deemed complete once the volume of the sample became constant.

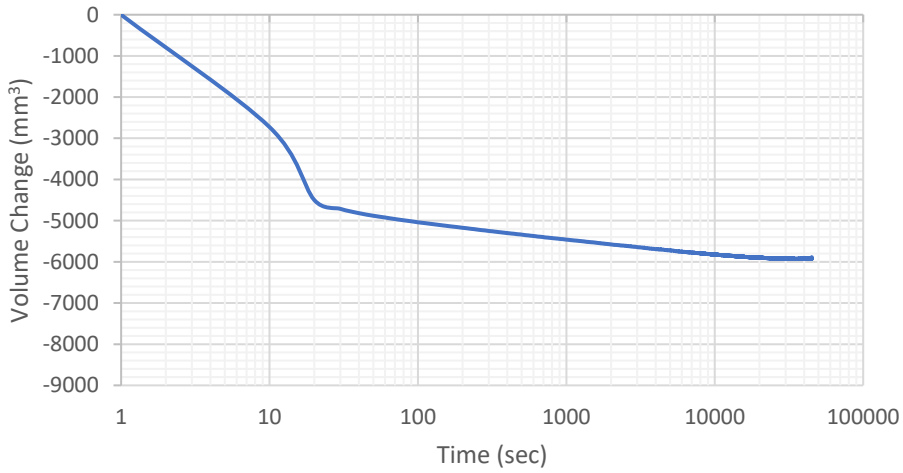

Figure 37: Consolidation curve for the second stage of specimen FM-D50-C1.2 (Table 5)

6.2 Stress-Strain Curves

Figures 39 through 41 show stress-strain curves for different shearing stages of tests on raw and FRS specimens.

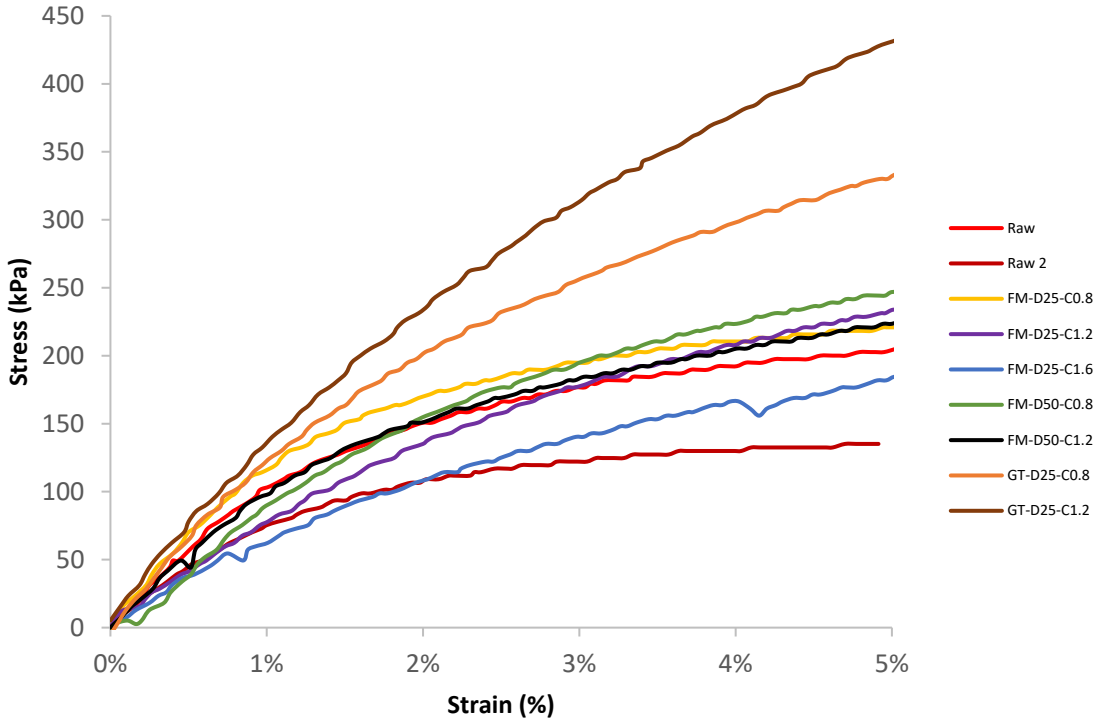

Figure 38: Stress strain curves for shearing stage 1

The first stage of shearing was conducted at a confining pressure of 50 kPa. The activation of the fiber reinforcements was clearly observed in the geotextile-reinforced specimens from the beginning to the end of this stage, resulting in toughness – represented by the area under each curve – values twice as large as those of the raw soil specimens. The data obtained in the interface shear tests conducted on the fiber materials suggested that the geotextile was more capable of interacting with the soil than the facemask at all considered confining pressures. Data in Figure 39 clearly demonstrate that the soil-fiber interaction of the geotextile material is more significant than that of the facemask

materials, as observed during the interface shear tests. The facemask FRS specimens did not exhibit distinct behaviour from the raw soil specimens until a strain level of 2% was reached. All FRS samples required higher levels of stress than unreinforced soil to achieve a strain of 5%. FM-D25-C1.6 was an exception to this, as it behaved similarly to raw soil specimens throughout this entire stage.

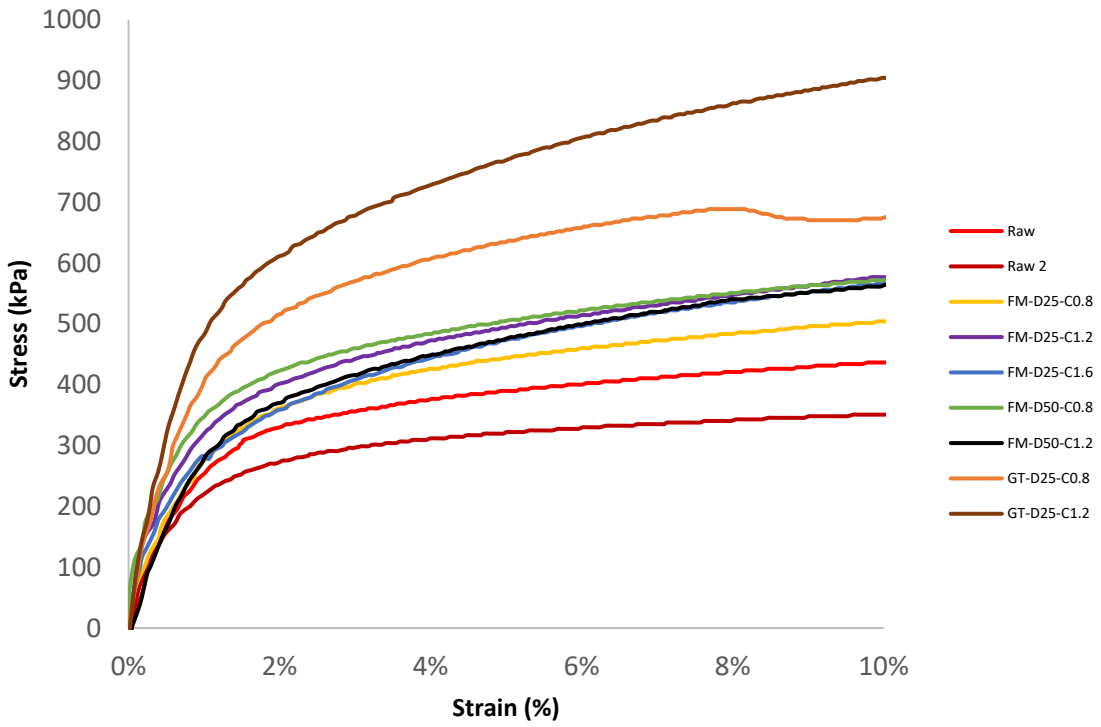

Figure 39: Stress-strain curves for shearing stage 2

More significant differences in the behaviour of the FRS specimens could be observed under an effective confining pressure of 250kPa in stage 2, as shown in Figure 40.

In Stage 2, all FRS specimens exhibited greater resistance to deformation when compared to the raw soil specimens. The activation of the fiber reinforcement elements became evident as soon as the samples underwent deformation, and the behaviour of FRS specimens was markedly distinct from that of the raw soil specimens. For facemask FRS specimens, an increased concentration of fiber reinforcement did not necessarily result in higher toughness. Specifically, specimen FM-D50-C0.8 outperformed FM-D50-C1.2, and FM-D25-C1.2 exhibited better performance than FM-D25-C1.6. Furthermore, FM-D25-C0.8 transitioned from being the toughest facemask FRS specimen in stage 1, to becoming the weakest FRS specimen in stage 2.

The final shearing stage, shown in Figure 41, was conducted under effective confining pressures of 450kPa. It is noteworthy that specimen FM-D25-C1.2 outperformed GT-D25-C0.8, displaying greater toughness and requiring a higher stress level to achieve a 15% strain. Notably, the activation of facemask fibers was slower compared to the geotextile specimen, as evidenced by the curves before reaching a 5% strain. One explanation for this behaviour is that the high volume of fibers, leading to a larger total area of soil-fiber interaction in the facemask specimen, outweighed the effects of the geotextile's higher strength and soil-fiber interaction coefficient.

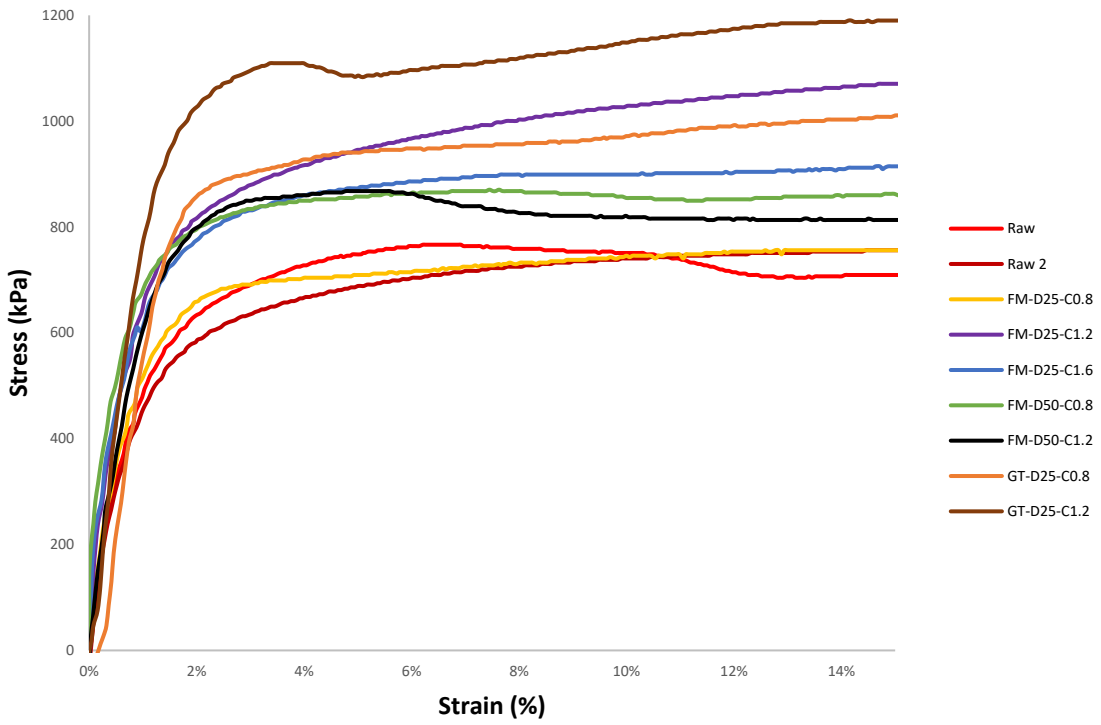

Figure 40: Stress-strain curves for shearing stage 3

However, a more appropriate comparison should be made between FM-D25-C1.2 and GT-D25-C1.2, as they share the same fiber reinforcement concentration. In this comparison, the geotextile still outperformed the facemask specimen, but the difference in the highest measured stress between the two decreased from a 400kPa gap in stage 2 to approximately 150kPa, indicating an improved performance of FM-D25-C1.2.

Following this, Table 15 presents the percentage change in maximum shear stress observed for the different FRS specimens at each stage.

Table 15: Maximum stress variations for FRS specimens [1]

Specimen	Maximum Stress (kPa)		
	Stage 1	Stage 2	Stage 3
RAW 1	205.3	436.6	766.6
RAW 2	135.1	350.8	756.1
FM-D25-C0.8	220.9 (+7.6%)	504.1 (+15.5%)	756.2 (-1.3%)
FM-D25-C1.2	233.9 (+13.9%)	576.9 (+32.1%)	1070.6 (+39.7%)
FM-D25-C1.6	184.5 (-10.1%)	566.5 (+29.8%)	914.7 (+19.3%)
FM-D50-C0.8	246.9 (+20.3%)	571.7 (+31%)	870.5 (+13.6%)
FM-D50-C1.2	223.5 (+8.9%)	563.9 (+29.2%)	867.9 (+13.2%)
GT-D25-C0.8	332.6 (+62%)	688.6 (+57.7%)	1010.8 (+31.9%)
GT-D25-C1.2	431.4 (+110.1%)	904.3 (+107.1%)	1190.1 (+55.3%)

[1] Percentages are based on Raw 1 values for each stage

From Table 15, it can be observed that the difference in the performance of the FRS specimens becomes less significant as progress through stages is made and the effective pressure in the triaxial cell increases. Indeed, GT-D25-C1.2 performed better than FM-D25-C1.2 by a margin of 96.2% in stage 1, but that decreased to 75 points and 15.6 points in stages 2 and 3, respectively; and also better than FM-D50-C1.2, being apart by 101.2, 77.9 and 42.1 percents in stages 1, 2 and 3, respectively. A similar trend can be observed for specimens

with concentrations of 0.8 kg/m^3, with the difference between geotextile and facemask fibers becoming less significant in more advanced stages.

Specimen FM-D25-C1.6 initially exhibited poorer performance compared to the raw soil during stage 1. However, as the test progressed into later stages, the effects of reinforcement became more apparent. Nonetheless, when compared to specimen Raw 2, the observed values still fell within the range of raw soil performance, suggesting minimal or no activation of the fiber reinforcement during this initial stage. The variations observed in the strength of this FRS specimen could be attributed to the soil preparation and compaction processes, which might have played a role in low confining pressure conditions, like those of stage 1, but stopped being an issue in consecutive stages.

As evident from some stress-strain curves like that of specimen GT-D25-C0.8 in stage 2, or specimens Raw 1 and FM-D50-C1.2 in stage 3, it is noticeable that the curves do not always exhibit a consistent upward trend or comparable shape. Some specimens display significant stiffness at lower strain levels, which diminishes as strain increases. This phenomenon may be attributed to the internal rearrangement of particles induced by stress, leading to the activation or formation of planes of weakness within the soil structure. Consequently, this variability in curve shapes and peak values occurring at different strain levels can complicate the comparison of specimen performances.

An alternative method for assessing the performance of FRS specimens is by quantifying the total area beneath the strain-stress curves. This measurement offers valuable insights into the specimen's toughness, which represents its capacity to deform plastically without

fracturing. Evaluating toughness is especially relevant in applications where materials need to absorb energy and deform under varying loads, which are relevant for FRS applications such as slope reinforcement. The areas under the strain-stress curves depicted in Figures 39 to 41 are graphical representations of the toughness exhibited by each specimen during triaxial testing. Figure 42 presents these toughness values in both graphical and tabular formats.

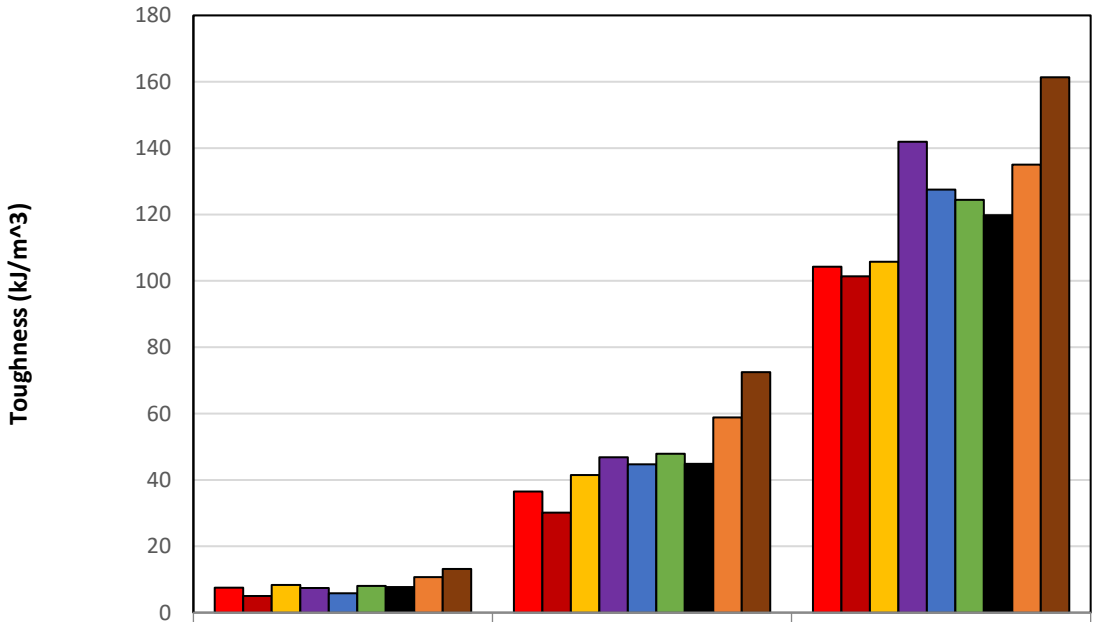

	Stage 1	Stage 2	Stage 3
Raw	7.51	36.50	104.27
Raw 2	5.01	30.16	101.37
FM-D25-C0.8	8.37	41.46	105.78
FM-D25-C1.2	7.43	46.82	141.94
FM-D25-C1.6	5.86	44.71	127.53
FM-D50-C0.8	8.06	47.91	124.41
FM-D50-C1.2	7.72	44.84	119.79
GT-D25-C0.8	10.73	58.86	135.04
GT-D25-C1.2	13.17	72.49	161.33

Figure 41: Toughness of FRS Specimens

The results for "Raw Soil" and "Raw Soil 2" in Figure 42 provide benchmark toughness values for the raw sand. Results also indicate that different types and concentrations of fiber has led to varying degrees of enhancement in the toughness of FRS specimens.

In Stage 1, distinctions in toughness are subtle. Notably, specimens reinforced with geotextile materials exhibit a discernible uptick in toughness. This trend is less pronounced in the case of facemask-reinforced specimens, which do not deviate significantly from the observations made on raw soil specimens during this stage.

Stage 2 unveils more pronounced differences in toughness characteristics. Here, the geotextile-reinforced specimens distinctly outperform all other variants, displaying a higher toughness. In contrast, the facemask-reinforced specimens, while exhibiting improvement in toughness compared to the baseline raw soil, do so in a more moderate manner.

In Stage 3, the reinforcement effects become even more evident for both geotextile and facemask-reinforced specimens when contrasted with the unaltered raw soil specimens. During this stage, it is observed that the higher effective compressive strength due to soil-fiber interaction can lead to improved toughness and overall performance.

Figure 43 shows a comparison of normalized shear strength of the raw soil and FRS specimens. The strength values were obtained by dividing the maximum shear stress for each stage by the corresponding confining pressure.

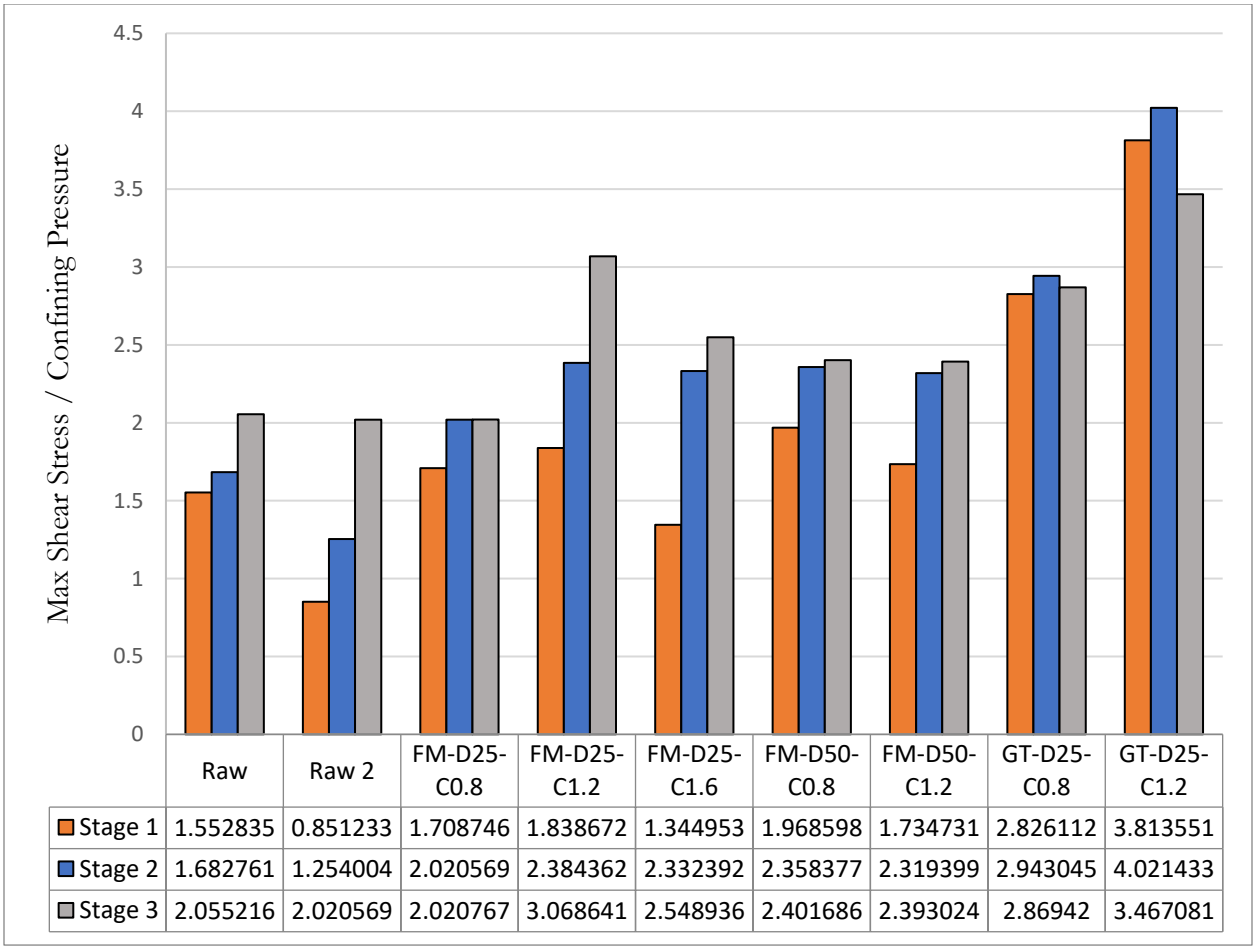

	Raw	Raw 2	FM-D25-C0.8	FM-D25-C1.2	FM-D25-C1.6	FM-D50-C0.8	FM-D50-C1.2	GT-D25-C0.8	GT-D25-C1.2
Stage 1	1.552835	0.851233	1.708746	1.838672	1.344953	1.968598	1.734731	2.826112	3.813551
Stage 2	1.682761	1.254004	2.020569	2.384362	2.332392	2.358377	2.319399	2.943045	4.021433
Stage 3	2.055216	2.020569	2.020767	3.068641	2.548936	2.401686	2.393024	2.86942	3.467081

Figure 42: Normalized Shear Strength of Raw Soil and FRS Specimens

6.3 Stiffness

The stress-strain curves of tested specimens in Figures 39 to 41 were also used to determine their initial tangent modulus of elasticity, as a measure of their stiffness as a function of fiber concentration. The resulting values are listed in Table 16 and Figure 44.

Table 16: Young's Modulus of tested specimens based on the initial linear segment of their mechanical response in Figs. 38-40

Specimen	Young's Modulus (kPa)		
	Stage 1	Stage 2	Stage 3
RAW 1	77.95	214.38	307.98
RAW 2	63.39	155.93	292.75
FM-D25-C0.8	93.28	222.71	329.57
FM-D25-C1.2	72.72	205.94	393.17
FM-D25-C1.6	46.64	190.12	336.47
FM-D50-C0.8	98.32	239.34	311.19
FM-D50-C1.2	84.6	259.85	448.56
GT-D25-C0.8	103.95	324.8	674.94
GT-D25-C1.2	118.77	423.02	654.44

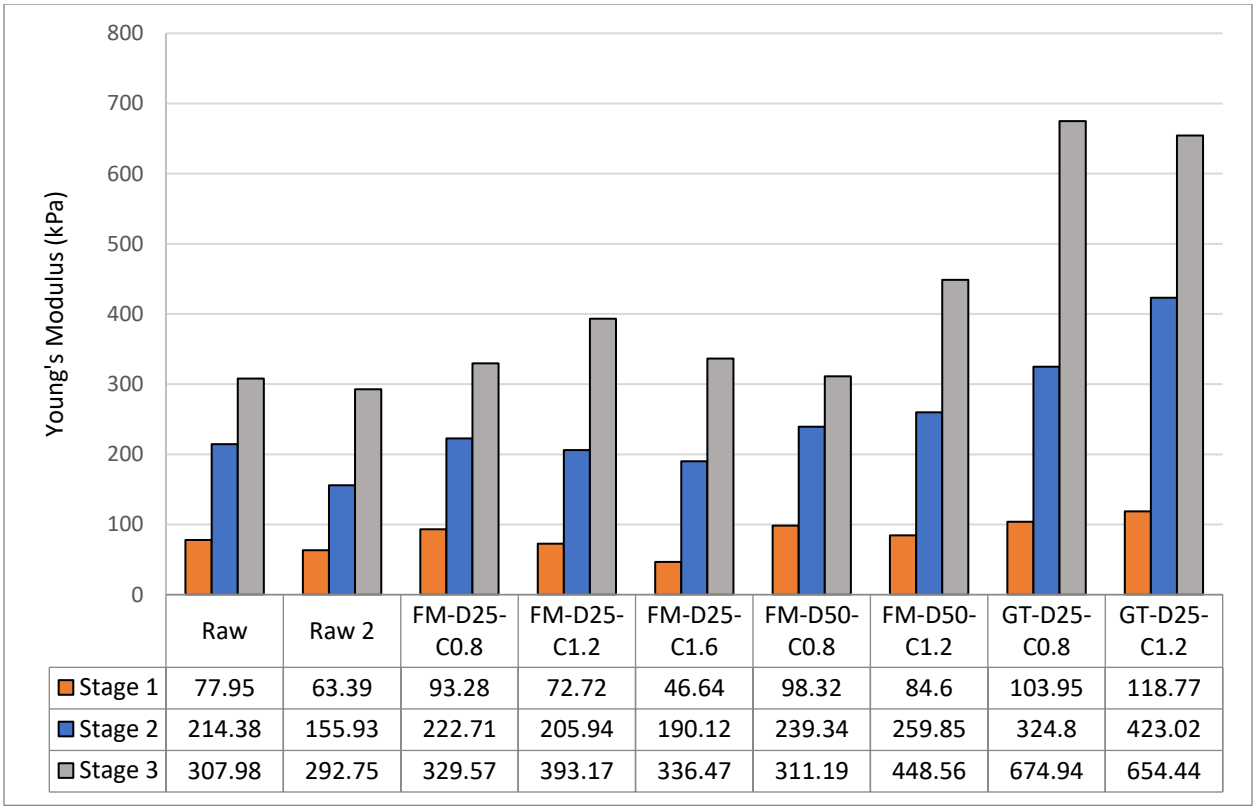

	Raw	Raw 2	FM-D25-C0.8	FM-D25-C1.2	FM-D25-C1.6	FM-D50-C0.8	FM-D50-C1.2	GT-D25-C0.8	GT-D25-C1.2
Stage 1	77.95	63.39	93.28	72.72	46.64	98.32	84.6	103.95	118.77
Stage 2	214.38	155.93	222.71	205.94	190.12	239.34	259.85	324.8	423.02
Stage 3	307.98	292.75	329.57	393.17	336.47	311.19	448.56	674.94	654.44

Figure 43: Young's Modulus of tested specimens based on the initial linear segment of their mechanical response in Figs. 38-40

6.4 Cohesion and Friction Angle

Figure 45 shows an example plot for a face mask FRS specimen. Strength envelopes for all FRS specimens are provided in Appendix A.

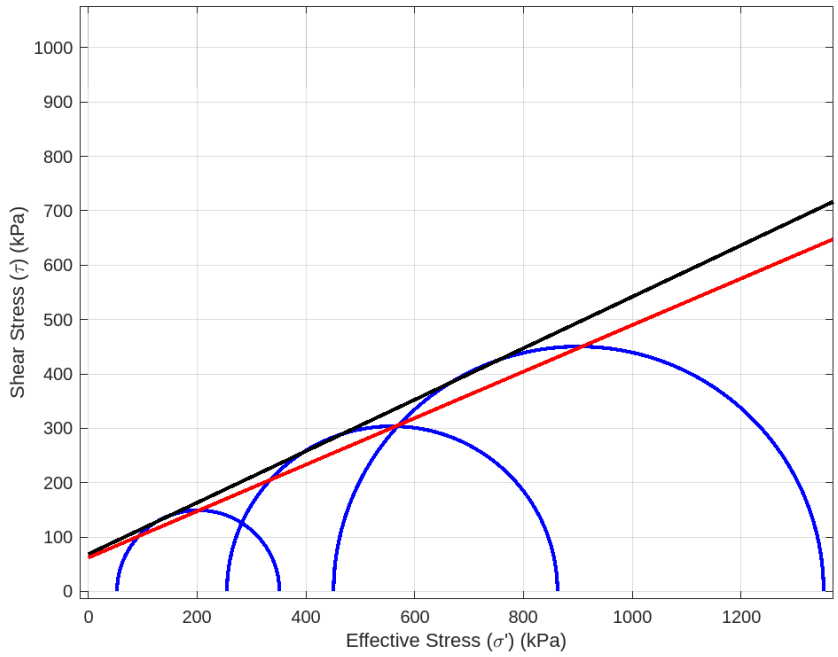

Figure 44: Strength envelopes for FM-D50-C0.8 (effective stress)

The cohesion value was determined by finding the y-intercept of the tangent line, while the friction angle was calculated as the angle formed between the tangent line and the x-axis. Table 17 shows calculated values of cohesion and friction angle for both the total and effective strength envelopes. The table also includes results predicted by Dr. Gregory's model, which is discussed in Appendix B, and percentage change of each parameter in reference to raw soil measurements. The tabulated data in Table 17 are also plotted in Figures 46 and 47.

Table 17: Calculated values of cohesion and friction angle for different specimens from triaxial tests (with percentage changes[2])

Specimen	Total		Effective		Predicted effective value using Gregory's model (2006)[1]	
	c (kPa)	ϕ (degrees)	c' (kPa)	ϕ' (degrees)	c* (kPa)	ϕ* (degrees)
Raw 1	0	36.0	47.5	24.0	-	-
Raw 2	36.2	25.1	81.6	24.0	-	-
Raw Average	18.1	30.6	64.6	24.0	-	-
FM-D25-C0.8	53.8 (+197%)	13.7 (-55%)	87.3 (+35%)	11.6 (-52%)	52 (-19%)	24.6 (+3%)
FM-D25-C1.2	0 (-100%)	29.4 (-4%)	11.9 (-82%)	24.4 (+2%)	54.2 (-16%)	24.9 (+4%)
FM-D25-C1.6	26.9 (+49%)	27.3 (-11%)	42.9 (-34%)	28.3 (+18%)	56.5 (-13%)	25.3 (+5%)
FM-D50-C0.8	24.8 (+37%)	26.6 (-13%)	68.6 (+6%)	25.1 (+5%)	50.7 (-22%)	24.4 (+2%)
FM-D50-C1.2	25.6 (+41%)	25.5 (-17%)	60.2 (-7%)	25.3 (+5%)	52.3 (-19%)	24.7 (+3%)
GT-D25-C0.8	0 (-100%)	29.4 (-4%)	2.7 (-96%)	24.4 (+2%)	47.8 (-26%)	24.3 (+1%)
GT-D25-C1.2	48.7 (+169%)	27.9 (-9%)	104.9 (+63%)	28.7 (+20%)	47.9 (-26%)	24.4 (+2%)

[1] Based on average of Raw 1 effective values

[2] Percentages based on average of Raw 1 and Raw 2 values

In Table 17, the data related to FRS specimens can be divided into three main sections. The first section presents the total cohesion and friction angle values in the initial two columns. Following that, the central two columns provide information about effective cohesion and friction angle. Lastly, the last section of the table displays predictions of effective cohesion and friction angle, calculated using a mathematical model developed by Gregory (2006). Parameters calculated based on effective stress are of greater significance when assessing soil performance. This is because they exclude the influence of water in resisting shearing stress, allowing for a more accurate quantification of the soil's inherent behavior.

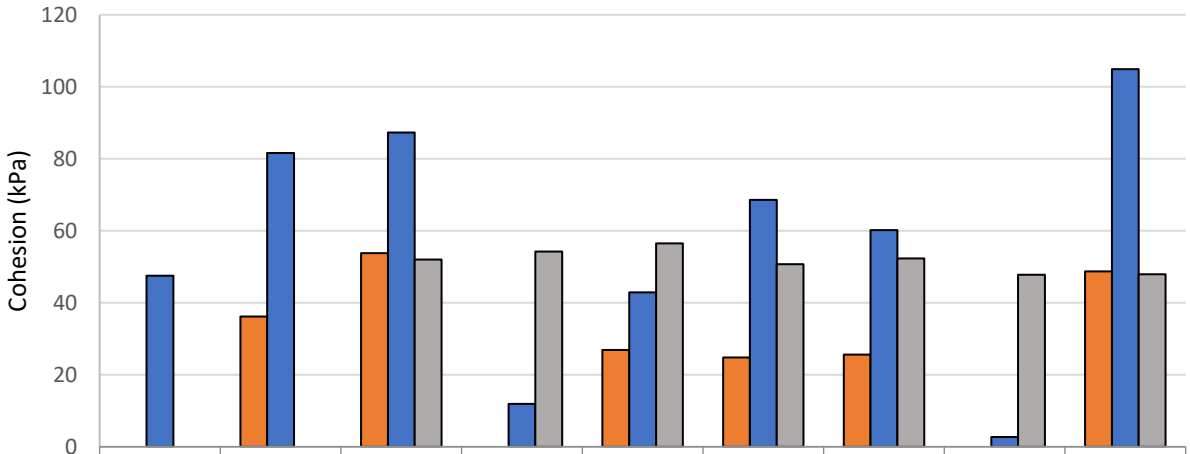

	Raw 1	Raw 2	FM-D25-C0.8	FM-D25-C1.2	FM-D25-C1.6	FM-D50-C0.8	FM-D50-C1.2	GT-D25-C0.8	GT-D25-C1.2
c	0	36.2	53.8	0	26.9	24.8	25.6	0	48.7
c'	47.5	81.6	87.3	11.9	42.9	68.6	60.2	2.7	104.9
c*	0	0	52	54.22	56.5	50.7	52.3	47.8	47.9

Figure 45: Calculated values of cohesion for Raw Soil and FRS specimens

Figure 46 illustrates the estimated cohesion values for each specimen. In general, there is a consistent trend regarding the average effective cohesion of FRS specimens, which is a reduction when compared to the effective cohesion of the raw soil. Interestingly, specimens with larger fibers measuring 5.1 x 51 mm (D50) exhibit a relatively smaller effect on effective cohesion, leading to less significant variations compared to specimens with smaller fibers measuring 2.58 x 51 mm (D25). Fiber concentration does not appear to consistently influence the cohesion of the soil. Predictions based on Gregory's model, suggest an increase in effective cohesion with the introduction of reinforcements.

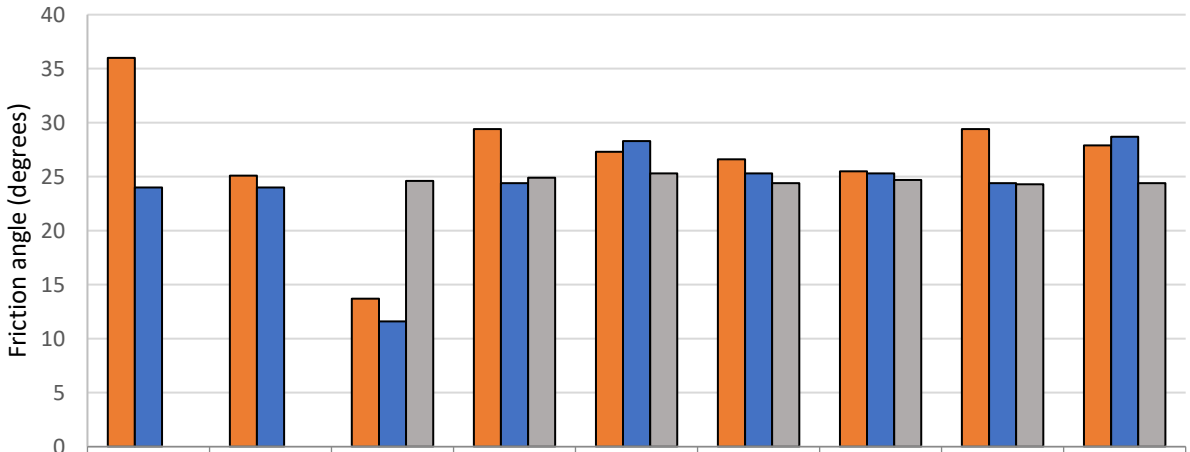

	Raw 1	Raw 2	FM-D25-C0.8	FM-D25-C1.2	FM-D25-C1.6	FM-D50-C0.8	FM-D50-C1.2	GT-D25-C0.8	GT-D25-C1.2
ϕ	36	25.1	13.7	29.4	27.3	26.6	25.5	29.4	27.9
ϕ′	24	24	11.6	24.4	28.3	25.3	25.3	24.4	28.7
ϕ*	0	0	24.6	24.9	25.3	24.4	24.7	24.3	24.4

Figure 46: Calculated values of Friction angle for Raw Soil and FRS specimens

Conversely, as observed in Figure 47, there is a discernible increase in the effective friction angle among FRS specimens in comparison to values observed in the raw soil. Notably, fiber concentration emerges as a significant contributing factor to the variation

of this parameter, with specimens featuring higher concentrations of reinforcement consistently displaying higher effective friction angles. Furthermore, it is worth noting that fibers with larger dimensions exhibit a comparatively less pronounced increase in friction angle with the escalation of fiber concentration. The predictions of Gregory's model anticipate an increase in the friction angle, and the empirical data consistently surpasses the model's expectations.

Having identified the general trends in the data, it is notable that specimen FM-D25-C0.8 exhibits behavior that diverges from the expected patterns seen in the dataset. Unlike the typical trends, this specimen demonstrates a significant increase in effective cohesion and a marked decrease in the effective friction angle. The underlying causes for this deviation are not immediately evident. Potential factors could include variations in the distribution of fibers within the sample, potentially leading to the creation of planes of weakness. Indeed, this deviation from the overall data trend can be easily noticed in Figures 48 and 49, which show the total stress and the effective stress paths of each specimen, respectively.

The paths show three steps that correspond to each of the shearing stages of the triaxial test. In both the total and effective stress scenarios, a notable pattern emerges across most facemask-reinforced specimens: the increase from step 2 to step 3 is more pronounced than the change from step 1 to step 2. This phenomenon can be attributed to an enhanced soil-fiber interaction, likely stemming from the augmented confining pressure applied to the specimen. However, it is worth noting that FM-D25-C0.8 stands out from this trend,

displaying less substantial increases in the vertical axis values as the horizontal values increase, thereby deviating from the observed pattern.

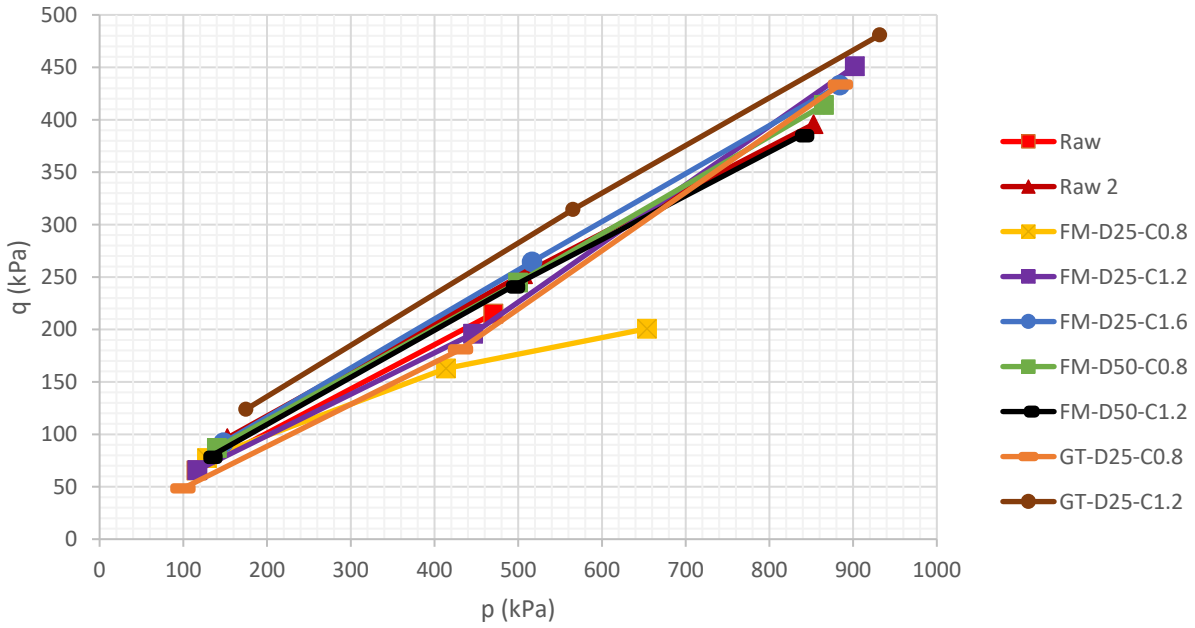

Figure 47: Total stress paths for tested specimens

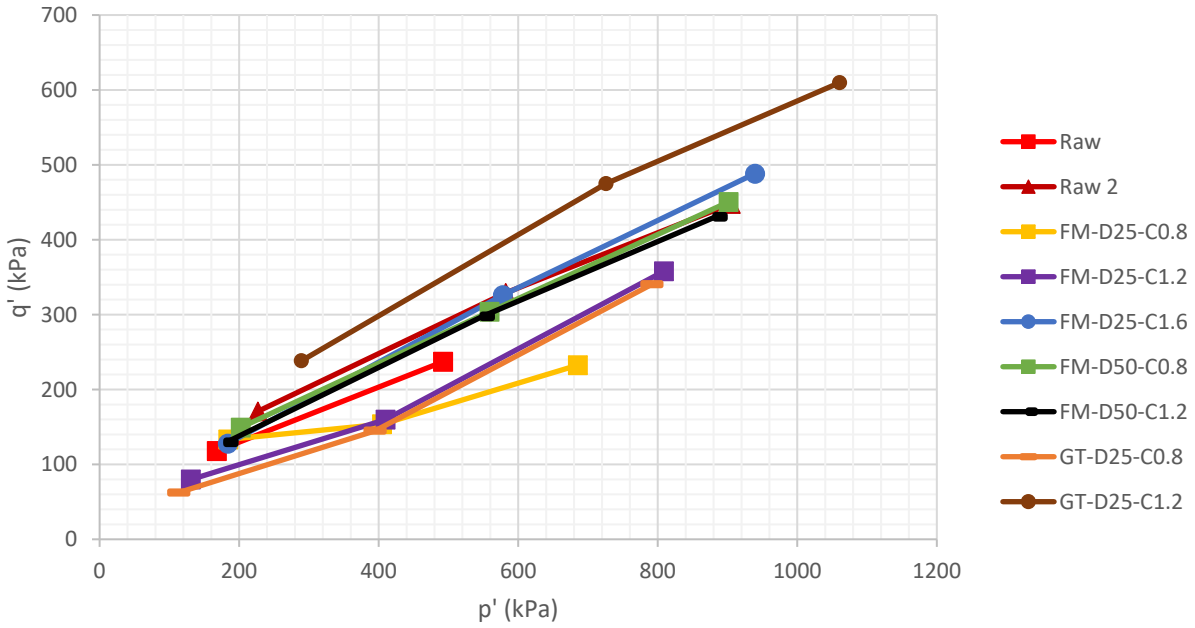

Figure 48: Effective stress paths for tested specimens

6.5 Dry Weight of Triaxial Specimens

The scatter observed in the shear strength data for raw soil specimens in Figures 39 to 41 indicate a possible omission in their preparation. The shear strength of soils is related to their unit weight. Even though a consistent compaction process was used to prepare all soil specimens, their unit weight was not measured and controlled during their preparation prior to the triaxial tests. As a result, observed differences in the shear strength of raw soil and FRS specimens may partly be due to the difference in the specimens' unit weight aside from the influence of facemask fiber reinforcement. Fortunately, all soil specimens were saved in sealed plastic bags following each triaxial test, which made it possible to determine their weight after the fact, with the results as shown in Table 18. All specimens were oven dried following the ASTM D2216 test protocol.

Table 18: Dry Unit Weights of Triaxial Specimens After the Tests

Specimen	Dry Mass (grams)	Dry Unit Weight[(1)] (kN/m^3)
Raw 1	1,055	18.40
Raw 2	907	15.82
FM-D25-C0.8	1,041	18.16
FM-D25-C1.2	1,068	18.63
FM-D25-C1.6	1,087	18.96
FM-D50-C0.8	1,036	18.07
FM-D50-C1.2	1,022	17.83
GT-D25-C0.8	1,015	17.71
GT-D25-C1.2	1,051	18.33

(1) Based on the triaxial test mold volume of 2248 cm^3.

Chapter 7 – Analysis of Results

7.1 Unit weight of soil specimens

The weight results for triaxial test specimens confirm that 'Raw 2' specimen's weaker response relative to 'Raw 1' could be explained by its significantly lower unit weight. Its unit weight was also inconsistent with those of FRS specimens. Therefore, data from this specimen was not included in the analysis of results presented in the subsequent sections. Accordingly, the values of mean, standard deviation, and Coefficient of Variation (CoV) of dry mass across all specimens as reported in Table 18 were calculated as 1,047 grams, 22.6 grams, and 2.16% respectively. The corresponding values of mean, standard deviation and CoV for the soil unit weight were 18.26 kN/m^3, 0.39 kN/m^3 and 2.15%, respectively.

The above results indicate that the variation in unit weight of the specimens (excluding Raw 2 soil) was within a 5% range from the mean value, which is considered acceptable per the FHWA in terms of compaction consistency (e.g. Berg et al. 2009). Therefore, the observed differences in mechanical performance of raw vs. FRS specimens as reported and discussed in this study (aside from the case of Raw 2 specimen) are not believed to be due to differences in specimen unit weight to a significant extent.

7.2 Soil Stiffness

As exhibited in Figures 39 to 41, the significantly lower soil strength relative to that of the raw soil in the case of specimen FM-D25-Co.8 is considered an anomaly in the results. Stress paths and toughness of this specimen also deviate from the trends observed in all

other specimens. Issues in sample preparation such as inadequate compaction, fiber distribution leading to the formation of weak planes, or undetected membrane leaks or equipment issues during triaxial testing may have been among possible factors leading to inconsistent results. Due to these inconsistencies, this specimen was excluded from further analysis and was classified as an outlier.

Comparison of the results shown in Figure 43 indicates that the facemask reinforcement led to some increase in stiffness compared to raw soil. However, the extent of improvement was not as significant as that in geotextile-reinforced specimens. Other specimens such as FM-D25-C1.2 and FM-D25-C1.6 initially displayed lower stiffness values compared to the raw soil, demonstrating changes of -7% and -40% for Stage 1 and -4% and -11% for Stage 2, respectively. However, a shift occurred in Stage 3, where these specimens showed an increase in stiffness by 27% and 9%, respectively.

The D50 specimens consistently exhibited an improvement in stiffness across all stages of testing. Observed increases in compressive stiffness in Specimen FM-D50-C0.8were 26%, 11%, and 1% for Stages 1, 2, and 3, respectively. Corresponding increases for FM-D50-C1.2 were 9%, 21%, and 46% for the respective stages. A comparison between the magnitudes of increase in compressive stiffness between D25 and D50 specimens confirms that D50 FRS specimens involved greater increases in the soil compressive stiffness, as shown on Figure 44.

7.3 Soil Strength

The first objective of this study was to demonstrate the improvement in soil shear strength due to shredded facemask fibers in the form of Fiber-Reinforced Soils (FRS). This objective was fulfilled by the results obtained across all shearing stages. In the initial phase at 50 kPa confining pressure, facemask-reinforced FRS specimens exhibited an 8% increase in shear strength, with an average increase of approximately 49.7 kPa when compared to unreinforced raw soil. This improvement continued in stage 2, conducted at 250 kPa effective confining pressure, showing an average of 27.5% increase, with an average improvement of 162.9 kPa in maximum shear strength. The improvement in strength extended into stage 3, carried out at 450 kPa effective confining pressure, demonstrating an average of 16.9% increase, with an average shear strength improvement of approximately 134.6 kPa in FRS specimens.

The second objective was to examine the influence of selected facemask fiber attributes on the shear strength of Fiber-Reinforced Soils (FRS). The attributes of interest at this stage were the fibers' concentration and dimensions. Results shown in Figs. 38 to 41 and Table 15 show that fiber concentration can have a significant influence on the FRS shear strength. For example, there is a consistent trend across all three stages, where FM-D25-C1.2 outperformed FM-D25-C1.6, and FM-D50-C0.8 exhibited greater strength compared to FM-D50-C1.2. This suggests that these higher concentrations of fibers tested were past the optimum level for that given aspect ratio, explaining why lower concentrations delivered better performance. Also, as evidenced in the toughness analysis of the specimens, aspect ratio was an discerning factor between fiber groups, as the thinner D25

specimens demonstrated a higher shear strength than D50 specimens. For example, in the second stage, the FM-D25-C1.2 specimen showed an increase in shear strength of approximately 32.1%, while the corresponding increase in FM-D50-C1.2 was 29.2%, which suggests a slight advantage for the 25 mm fibers. This better performance became definitive in the third stage, where the D25 specimen showed a 39.7% improvement compared to a 13.2% of the D50 case.

This led to the third objective of the study, which was to determine a practically optimum combination of fibers' aspect ratio and concentration to maximize FRS shear strength within the limited scope of the study. Results showed that overall, thinner and longer facemask fibers led to more desirable soil properties. This is corroborated by the higher strength and toughness values obtained for the D25 specimens, particularly in Stages 2 and 3 of the CUIC triaxial tests. However, D50 specimens also showed improved performance compared to raw soils and overall, within the ballpark of the performance observed from D25 specimens. Meanwhile, their effective cohesion values were overall greater than those obtained for D25 specimens and at the same time showed a 5% improvement in the effective friction angle. Thus, the concept of practically optimum fiber concentration requires further testing and analysis to produce clearer trends and outcomes in the continuation of this study.

Results of the study (e.g. data presented in Figs. 38 to 40 and Tables 15 and 17) also indicated that the range of fiber concentrations for the materials and aspect rations examined likely encompassed optimal fiber concentration in the corresponding cases. For instance, the toughness and shear strength of FM-D50 specimens were consistently at the

concentrations of 0.8 kg/m^3 were consistently greater than those for the 1.2 kg/m^3 alternative. Similarly, FM-D25 specimens performed better at the 1.2 kg/m^3 concentration than at 1.6 kg/m^3. In contrast, the performance of geotextile FRS specimens improved at higher concentrations, which confirms that optimal fiber concentration in FRS depends on the fiber material. According to the results of this study, optimal concentrations for the D25 and D50 facemask FRS specimens are 1.2 kg/m^3 and 0.8 kg/m^3, respectively.

Finally, this study was bound by several limitations as outlined below:

(1) the fabrication of fibers was a manual process, which imposed constraints on the production of very thin strips of material, preventing the evaluation of thinner aspect ratios. (2) the time and preparation required to set up and carry out the triaxial tests limited the number of experiments that could be carried out withing the period of this study. As a result, the variations in the number of factors that could be investigated were limited. Moreover, this limitation hindered the number of repeat tests to verify or modify the data for any test cases that were found to be inconsistent with other results (e.g. the results for FM-D25-C0.8 vs. FM-D50-C0.8 specimens mentioned earlier in this chapter).

(3) The raw soil was a blend of fine sand and industrial limestone, which was produced for efficacy of testing and analysis. Care must be taken in extending the results of study to other soils in the field even with comparable gradation. Further testing and verifications are necessary to apply the quantitative results of the study to various field projects.

7.4 Total Strain of Triaxial Specimens

After reviewing the procedures post-triaxial testing, it became evident that the applied levels of strain on each specimen exceeded the recommended thresholds outlined in the literature review and ASTM specifications. Contrary to the prescribed increment of 5% strain per stage amounting to a total of 15% strain, our testing protocol involved increments of 5%, 10%, and 15% strain per stage, culminating in a total strain of 30%. This departure from established practices, as recognized in prior experimental works known to the author, introduces a notable deviation. Consequently, this deviation raises uncertainties about the comparability of these results with those that might have been obtained through the conduction of triaxial tests adhering strictly to a single-stage approach. Additionally, the substantial strain levels imposed on the soil specimens have the potential to significantly alter their mechanical behavior and structural integrity. This excessive strain could induce excessively non-linear responses, potential failure mechanisms, and alterations in soil fabric not typically observed under lower strain conditions. Such deviation from the anticipated stress-strain behavior might lead to the development of atypical soil structures, shearing patterns, or even premature failure, thereby compromising the representativeness and reliability of the obtained results. Moreover, the excessive strain levels may obscure crucial insights into the soil's true mechanical properties under service conditions, rendering interpretations less conclusive and impeding the direct comparability of these findings to studies adhering to standard strain regimes.

Chapter 8 – Conclusions and Recommendations

8.1 Summary of Results

- Cylindrical raw and facemask-reinforced specimens, with a diameter of 71 mm and a height of 142 mm, underwent testing through the CUIC multistage triaxial test. The average dry soil unit weight of these tested specimens was recorded at 18.26 kN/m^3.

- Facemask fiber-reinforced specimens consistently exhibited an increase in effective friction angle, while either maintaining constant or reducing effective cohesion in FRS cases. Specimen FM-D25-C1.6 showed greatest amount of increase in friction angle by 18%, whereas FM-D50-C0.8 let to a 6% increase in effective cohesion, remaining the only case in the study where cohesion wasn't reduced.

- The incorporation of D25 facemask fibers into the soil led to a considerable amount of increase in the soil's shear strength, by as much as 39.5%. Furthermore, the stiffness of specimens that included these fibers showed a notable rise in their modulus of elasticity by as much as 27%.

- D50 facemask fibers also led to a substantial increase in the shear strength of the soil, with improvements of up to 31%. Additionally, these fibers significantly increased the stiffness of specimens by as much as 45%.

8.2 Conclusions

This research study examined possible improvements in soil properties through the use of facemask fibers in the form of Fiber-Reinforced Soils (FRS). Study results indicated that proper use of facemask fibers in soil can lead to an improvement in shear strength at

different deformation levels. Furthermore, the study highlighted the importance of fiber concentration and dimensions, (e.g. aspect ratio) on the magnitude of improvement in soil strength and stiffness. Within the limited number of combinations that was possible to investigate in this study, thinner (i.e. 25.4 mm wide) and longer fibers appeared to be slightly more effective in improving soil properties. Additionally, the data suggested that optimal fiber concentration varied with the fiber aspect ratio and material.

The practicality of implementing this form of reinforcement in various soil applications needs a separate study, and needs to iniclude several key considerations. A procedure needs to be developed to collect and recycle facemasks properly and effectively. They need to be reliably sanitized. Afterwards, the strongest layer as determined in this study needs to be separated and shredded in desired aspect ratios to ensure the viability and reliability of this FRS alternative.

One variation in the process outlined above could involve shredding the entire facemask into fibers to save time and costs. However, the efficacy of this approach in soil improvement, leading to more significantly variable fibers relative to their material type, size and strength than what was investigated in the current project needs to be examined in continuation of this study..

8.3 Recommendations for Future Work

To the best of the author's knowledge, this study was the first involving laboratory tests to determine the properties of raw soil and a candidate facemask material for the reinforcement element. The aim of this research was to establish a foundation for further

exploration and comprehension of the applicability of these materials in geotechnical engineering. Several variables need to be addressed to better understand the behavior of facemask materials as reinforcement elements.

First, it is crucial to examine the uniformity of facemask materials produced by different manufacturers. Variations in parameters such as material thickness and polymer composition may have a significant impact on the performance of the resulting reinforcement elements. Additionally, a comparison of material properties between used and new facemasks is necessary to assess the viability of recycled facemasks for FRS applications. These further investigations should consider factors such as the effects of humidity, temperature, and the stress history of discarded facemask materials, in addition to any disinfecting requirements.

Secondly, expanding the scope of testing to include more aspect ratios and configurations of facemask materials would yield a more comprehensive understanding of the most suitable formats for their application in FRS. Similarly, assessing the performance of facemask fiber materials in different soil types, such as clayey soils, is essential to determine their applicability in wider field applications.

Other types of triaxial test (e.g. UU or CD variations) could be carried out on different FRS specimens to examine their field applications under rapid loads (e.g. traffic) or in the long term.

Exploring the potential of hybrid FRS specimens, i.e. involving the use of both geotextile and facemask fibers, presents another avenue for further research. This approach allows

for the synergistic combination of different materials, offering the prospect of more cost-effective FRS applications.

In retrospect, the deviation from recommended strain increments in our triaxial testing revealed a departure from established standards, casting uncertainty over result comparability and reliability. The excessive strain imposed on soil specimens carries the potential to distort their mechanical behavior and compromise structural integrity, leading to atypical responses not reflective of true properties. To ensure future study reliability, adherence to standardized testing protocols, specifically in strain application, remains imperative. Future investigations should explore varying strain effects within prescribed thresholds, facilitating a comprehensive understanding of soil behavior under different loading conditions.

Bibliography

Abdullah, N. H. H., N. H. A. Aziz, F. F. Jaafar, N. M. Osman, A. Ahmad, and S. A. Hamid, 2019. "Effect of Different Fibre Reinforcement Type to the Shear Strength of Soft Soil at Varying Moisture Condition." Journal of Physics. Conference Series 1349.1: 12126. Web.

Ang, E.C., and J.E. Loehr, 2003. "Specimen Size Effects for Fiber-Reinforced Silty Clay in Unconfined Compression." Geotechnical Testing Journal 26.2: 1-10. Web.

Belkhatir, Mostefa, Ahmed Arab, Noureddine Della, and Tom Schanz, 2012. "Experimental Study of Undrained Shear Strength of Silty Sand; Effect of Fines and Gradation." Geotechnical and Geological Engineering 30.5: 1103-118. Web.

Belkhatir, Mostefa, Hanifi Missoum, Ahmed Arab, Noureddine Della, and Tom Schanz, 2011. "Undrained Shear Strength of Sand-silt Mixture: Effect of Intergranular Void Ratio and Other Parameters." KSCE Journal of Civil Engineering 15.8: 1335-342. Web.

Benziane, Mehdi Missoum, Noureddine Della, Sidali Denine, Sedat Sert, and Said Nouri, 2019. "Effect of Randomly Distributed Polypropylene Fiber Reinforcement on the Shear Behavior of Sandy Soil." Studia Geotechnica Et Mechanica 41.3: 151-59. Web.

Berg R.B., Christopher, B.R. and Naresh C. Samtani, 2009, “Design and Construction of Mechanically Stabilized Earth Walls and Reinforced Soil Slopes”, Volume I, Report No. FHWA-NHI-10-024, Federal Highway Administration, Washington, DC, USA.

Brand, E.W., 1976. "Back Pressure Effects on the Undrained Strength Characteristics of Soft Clay." International Journal of Rock Mechanics and Mining Sciences & Geomechanics Abstracts 13.5: 46. Web.

Consoli, Nilo Cesar, Michele Dal Toe Casagrande, and Matthew Richard Coop, 2005. "Effect of Fiber Reinforcement on the Isotropic Compression Behavior of a Sand." Journal of Geotechnical and Geoenvironmental Engineering 131.11: 1434-436. Web.

Correia, N.S., S.A. Rocha, P.C. Lodi, and J.S. McCartney, 2021. "Shear Strength Behavior of Clayey Soil Reinforced with Polypropylene Fibers under Drained and Undrained Conditions." Geotextiles and Geomembranes 49.5: 1419-426. Web.

Dissanayake, Janith, Cecilia Torres-Quiroz, Jyoti Mahato, and Junboum Park, 2021. "Facemasks: A Looming Microplastic Crisis." International Journal of Environmental Research and Public Health 18.13: 7068. Web.

Djafar Henni, Ahmed, Ahmed Arab, Mostefa Belkhatir, A. Saaed Hamoudi, and Hamid Khelafi, 2013. "Undrained Behavior of Silty Sand; Effect of the Overconsolidation Ratio." Arabian Journal of Geosciences 6.2: 297-307. Web.

Ehrlich, M., M.S.S. Almeida, and D. Curcio, 2019. "Hydro-mechanical Behavior of a Lateritic Fiber-soil Composite as a Waste Containment Liner." Geotextiles and Geomembranes 47.1: 42-47. Web.

Ekinci, Abdullah, Pedro Miguel Vaz Ferreira, and Mohammadreza Rezaeian, 2022. "The Mechanical Behavior of Compacted Lambeth-group Clays with and without Fiber Reinforcement." Geotextiles and Geomembranes 50.1: 1-19. Web.

ELE International. “Direct/Residual Shear Apparatus.” ELE International, www.ele.com/ProductGroup/direct-residual-shear-apparatus. Accessed 10 Oct. 2023.

Esmaili, Danial, 2014. A Study on Unsaturated Soil-geotextile Interface Strength Using Multi-scale Laboratory Tests / by Danial Esmaili. Web.

Feuerharmel, M.R., 2000. “Comportamento de Solos Reforçados com Fibras de Polipropileno.” Universidade Federal do Rio Grande do Sul (UFRGS), Porto Alegre (RS), p. 152 (in portuguese).

Ghiassian, Hossein, Gholamreza Poorebrahim, and Donald H. Gray, 2004. "Soil Reinforcement with Recycled Carpet Wastes." Waste Management & Research 22.2: 108-14. Web.

Giger, Silvio B., Russell T. Ewy, Valentina Favero, Rudy Stankovic, and Lukas M. Keller, 2018. "Consolidated-undrained Triaxial Testing of Opalinus Clay: Results and Method Validation." Geomechanics for Energy and the Environment 14: 16-28. Web.

Gregory, Garry H., 2006. “Shear Strength, Creep, and Stability of Fiber Reinforced Soil Slopes.” Oklahoma State University: 1-123. Web.

Janalizadeh Choobbasti, Asskar, and Saman Soleimani Kutanaei, 2017. "Effect of Fiber Reinforcement on Deformability Properties of Cemented Sand." Journal of Adhesion Science and Technology 31.14: 1576-590. Web.

Jaramillo, Natalia Andrea Durán, José Wilson Dos Santos Ferreira, José Adriano Cardoso Malko, and Michéle Dal Toé Casagrande, 2022. "Mechanical Behavior of Clayey Soil Reinforced with Recycled Tire Rubber Using Chips and Fibers." Geotechnical and Geological Engineering 40.6: 3365-378. Web.

Javdanian, Hamed, Navid Soltani, Gholamreza Shams, and Soroush Ghorbani, 2021. "Investigating the Monotonic Behavior of Fiber-reinforced Soil under Triaxial

Compression Using Experimental Modeling." Modeling Earth Systems and Environment 7.2: 943-52. Web.

Ji, Xiaolei, 2019. "GDS Triaxial Test on the Reinforcement Effects of Bermudagrass Root-soil Complex." IOP Conference Series. Earth and Environmental Science 304.3: 32106. Web.

Jia, Yu, Jia-sheng Zhang, Xuan Wang, Yu Ding, Xiao-bin Chen, and Tao Liu, 2022. "Experimental Study on Mechanical Properties of Basalt Fiber-reinforced Silty Clay." Journal of Central South University 29.6: 1945-956. Web.

Karimzadeh, Ali Akbar, Anthony Kwan Leung, Saied Hosseinpour, Zhaoyi Wu, and Pedram Fardad Amini, 2021. "Monotonic and Cyclic Behaviour of Root-reinforced Sand." Canadian Geotechnical Journal 99.999: 1915-927. Web.

Koerner RM. 2005. Designing with Geosynthetics. 5th ed., Pearson Prentice-Hall, Upper Saddle River, NJ, USA.

Li, Chunling, and Jorge G Zornberg, 2019. "Shear Strength Behavior of Soils Reinforced with Weak Fibers." Journal of Geotechnical and Geoenvironmental Engineering 145.9: Journal of Geotechnical and Geoenvironmental Engineering, 2019, Vol.145 (9). Web.

Lian, Baoqin, Jianbing Peng, Hongbin Zhan, and Xinsheng Cui, 2020. "Effect of Randomly Distributed Fiber on Triaxial Shear Behavior of Loess." Bulletin of Engineering Geology and the Environment 79.3: 1555-563. Web.

Lowe, John, Thaddeus C. Johnson, 1960. “Use Of Back Pressure To Increase Degree Of Saturation Of Triaxial Test Specimens.” ASCE Library

Nambiar, M. R. M., Rao, G. V., and Gulhati, S. K., "Multistage Triaxial Testing: A Rational Procedure," Strength Testing of Marine Sediments: Laboratory and In-Situ Measurements, ASTM STP 883, R. C. Chaney and K. R. Demars, Eds., American Society for Testing and Materials, Philadelphia, 1985, pp. 274-293.

Omar, Tarek. Specimen Size Effect On Shear Behavior of Loose Sand in Triaxial Testing (2013). Web.

Park, Sung-Sik, and Sueng Won Jeong. "Effect of Specimen Size on Undrained and Drained Shear Strength of Sand." Marine Georesources & Geotechnology 33.4 (2015): 361-66. Web.

Pradhan, Pradip Kumar, Rabindra Kumar Kar, and Ashutosh Naik. "Effect of Random Inclusion of Polypropylene Fibers on Strength Characteristics of Cohesive Soil." Geotechnical and Geological Engineering 30.1 (2012): 15-25. Web.

Rasouli, Habib, and Behzad Fatahi. "Liquefaction and Post-liquefaction Resistance of Sand Reinforced with Recycled Geofibre." Geotextiles and Geomembranes 50.1 (2022): 69-81. Web.

Rivera-Hernandez, Xavier A., Farshid Vahedifard, and Ghada S. Ellithy. "Effect of Suction and Confining Pressure on Shear Strength and Dilatancy of Highly Compacted Silty Sand: Single-Stage versus Multistage Triaxial Testing." Geotechnical Testing Journal 44.2 (2021): 407-21. Web.

StringKing. “How It's Made: Disposable 3-Layer Face Mask.” *StringKing*, https://stringking.com/face-masks/how-its-made-disposable-3-layer-face-mask/.

Saeidaskari, Javad, Mahdi Alibolandi, and Alireza Saeedi Azizkandi. "Undrained Monotonic and Cyclic Behavior of Qeshm Calcareous Sand." Marine Georesources & Geotechnology 39.7 (2021): 798-811. Web.

Schoenemann, Mark R., and Marvin R. Pyles. "Statistical Description of Triaxial Shear Test Results." Geotechnical Testing Journal 13.1 (1990): 58-62. Web.

Sobhan, Khaled, and Mehedy Mashnad. "Tensile Strength and Toughness of Soil-Cement-Fly-Ash Composite Reinforced with Recycled High-Density Polyethylene Strips." Journal of Materials in Civil Engineering 14.2 (2002): 177-84. Web.

Soltani, Amin, An Deng, Abbas Taheri, and Asuri Sridharan. "Swell–Shrink–Consolidation Behavior of Rubber–Reinforced Expansive Soils." Geotechnical Testing Journal 42.3 (2019): 761-88. Web.

Soranzo, M., "Results and Interpretation of Multistage Triaxial Compression Tests," Advanced Triaxial Testing of Soil and Rock, ASTM STP 977, Robert. T. Donaghe, Ronald C. Chaney, and Marshall L. Silver, Eds., American Society for Testing and Materials, Philadelphia (1988) pp. 353-362.

StringKing. “How It's Made: Disposable 3-Layer Face Mask.” StringKing (2021), https://stringking.com/face-masks/how-its-made-disposable-3-layer-face-mask/.

Sugiyama, Yuri, Katsuyuki Kawai, and Atsushi Iizuka. "Effects of Stress Conditions on B-value Measurement." Soils and Foundations 56.5 (2016): 848-60. Web.

Taha, Mazahir M. M., Cheng Pei Feng, and Sara H. S. Ahmed. "Influence of Polypropylene Fibre (PF) Reinforcement on Mechanical Properties of Clay Soil." Advances in Polymer Technology 2020 (2020): 1-15. Web.

Trafton, Anne. “The Environmental Toll of Disposable Masks.” MIT News | Massachusetts Institute of Technology, MIT News Office, 20 July 2021, https://news.mit.edu/2021/covid-masks-environment-0720#:~:text=All%20of%20those%20masks%20carry,of%20which%20is%20disposable%20masks.

Trindade, T. P. da, Iasbik, I., Lima, D. C. de, Minette, E., Silva, C.H. de C., Carvalho, C. A. B. de, Bueno, B. de S., Machado, C.C., 2006. Estudos laboratoriais do comportamento de um solo residual arenoso reforçado com fibras de polipropileno, visando `a aplicaç˜ao em estradas florestais. Rev. ´Arvore 30 (2), 215–222.

Wu, Ruiqian, Guang Yang, Shaohe Li, and Qichen Xiang. "Experimental Study on the Effects of Matric Suction on Shear Properties of Polypropylene Fiber Reinforced Unsaturated Clay." Materials 15.22 (2022): 8223. Web.

Yaghoubi, Ehsan, Arul Arulrajah, Mohammadjavad Yaghoubi, and Suksun Horpibulsuk. "Shear Strength Properties and Stress–strain Behavior of Waste Foundry Sand." Construction & Building Materials 249 (2020): 118761. Web.

Yarbaşı, Necmi. "The Freezing-thawing Behavior of Clayey Soils Reinforced with Scrap Tires Pieces." Mühendislik Bilimleri Dergisi 22.6 (2016): 559-62. Web.

Zhang, Tao, Guojun Cai, and Weihong Duan. "Strength and Microstructure Characteristics of the Recycled Rubber Tire-sand Mixtures as Lightweight Backfill." Environmental Science and Pollution Research International 25.4 (2018): 3872-883. Web.

Zhou, Yun-Yan, and Xiao-Mei Wang. "Mesomechanics Characteristics of Soil Reinforcement by Plant Roots." Bulletin of Engineering Geology and the Environment 78.5 (2019): 3719-728. Web.

Appendix A – Strength Envelopes from Triaxial Tests

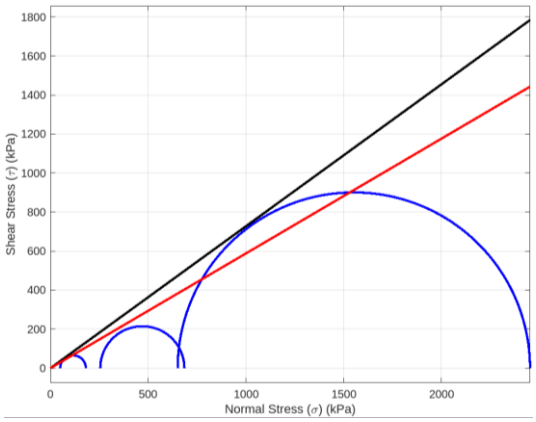

Figure 49: Raw 1 total stress

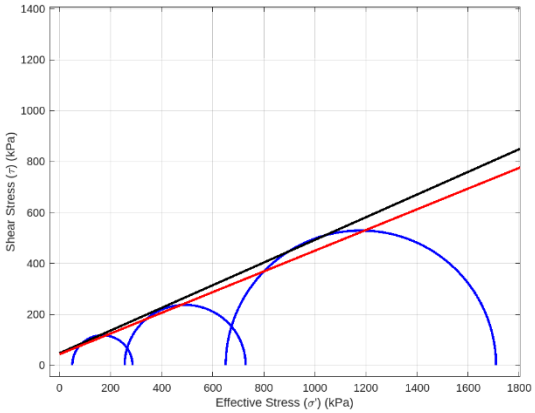

Figure 50: Raw 1 effective stress

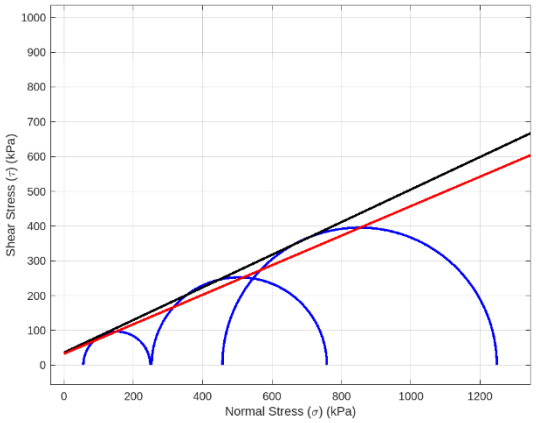

Figure 51: Raw 2 total stress

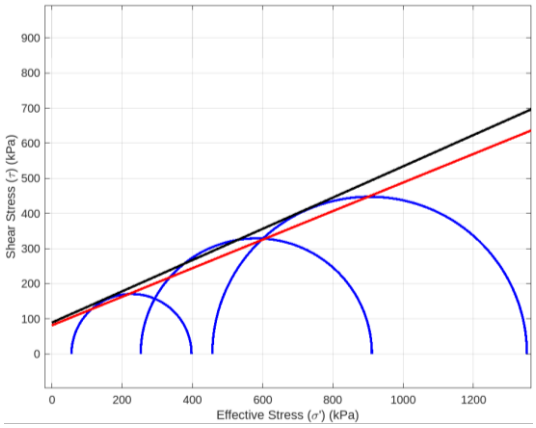

Figure 52: Raw 2 effective stress

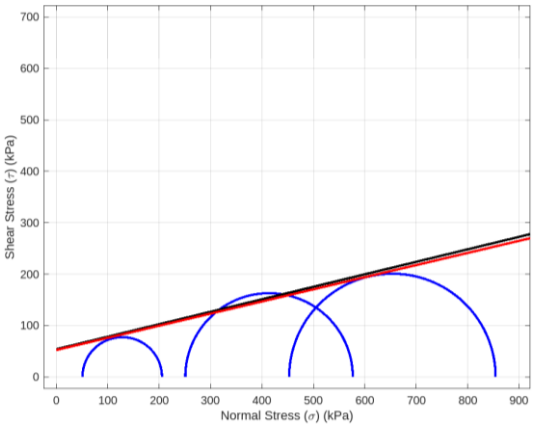

Figure 53: FM-D25-Co.8 total stress

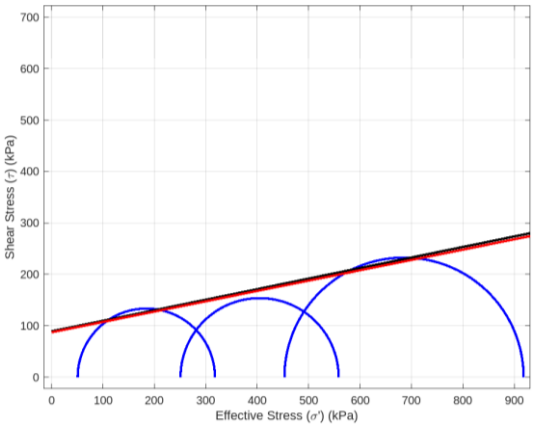

Figure 54: FM-D25-Co.8 effective stress

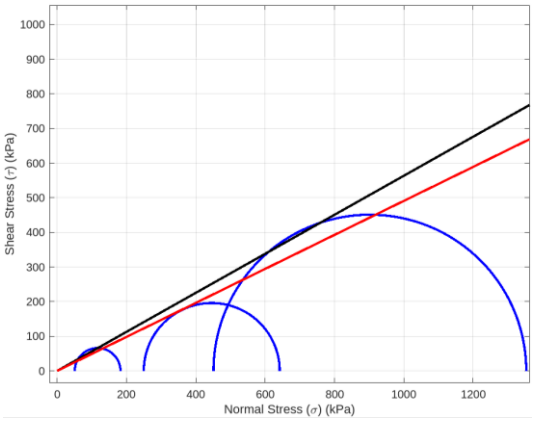

Figure 55: FM-D25-C1.2 Total Stress

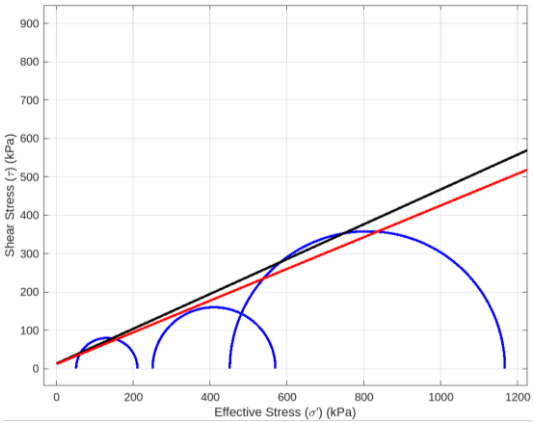

Figure 56: F-D25-C1.2 Effective Stress

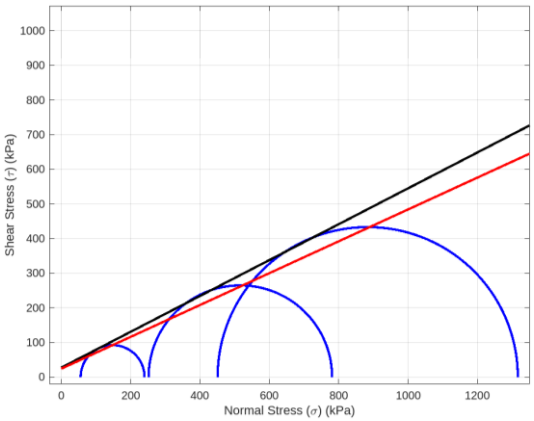

Figure 57: FM-D25-C1.6 total stress

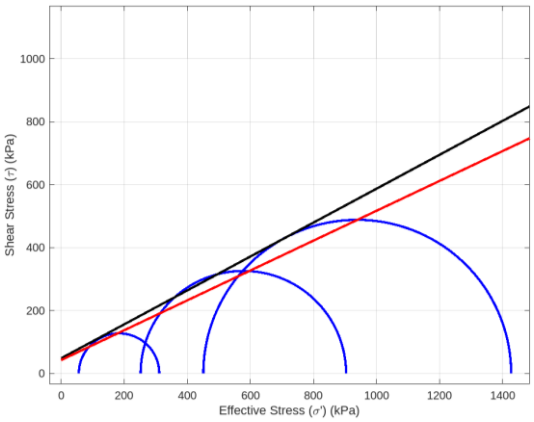

Figure 58: FM-D25-C1.6 effective stress

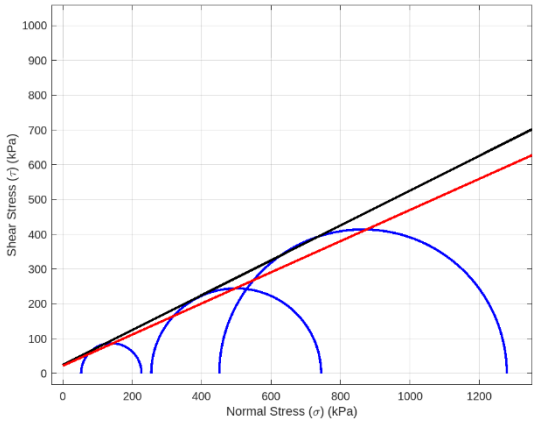

Figure 59: FM-D50-Co.8 total stress

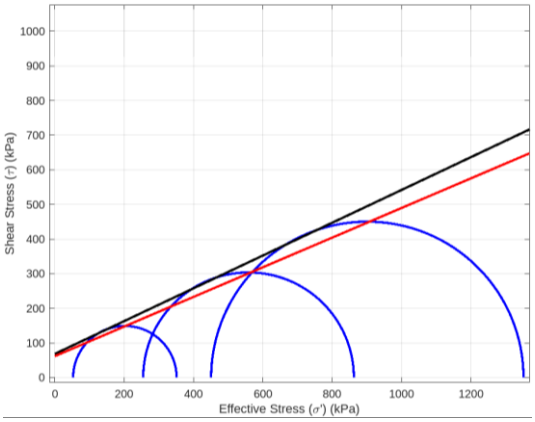

Figure 60: FM-D50-Co.8 effective stress

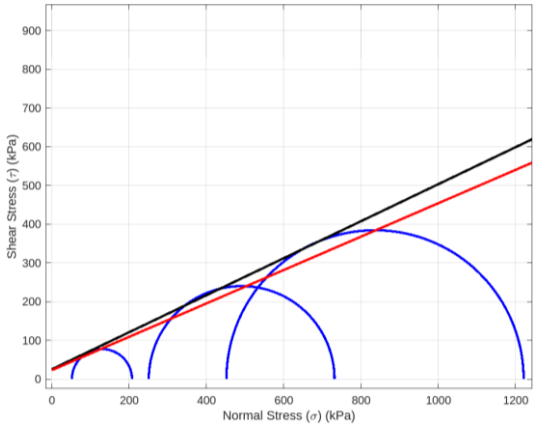

Figure 61: FM-D50-C1.2 Total Stress

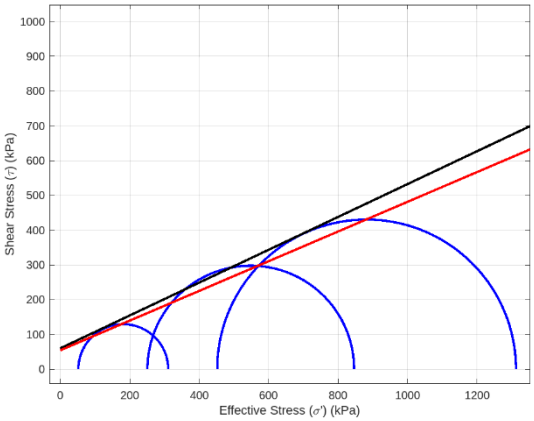

Figure 62: FM-D50-C1.2 Effective Stress

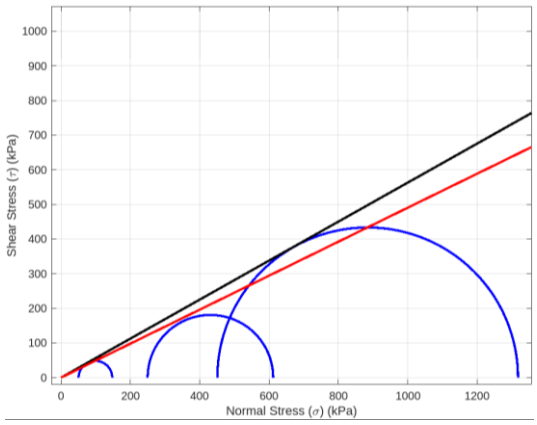

Figure 63: GT-D25-Co.8 total stress

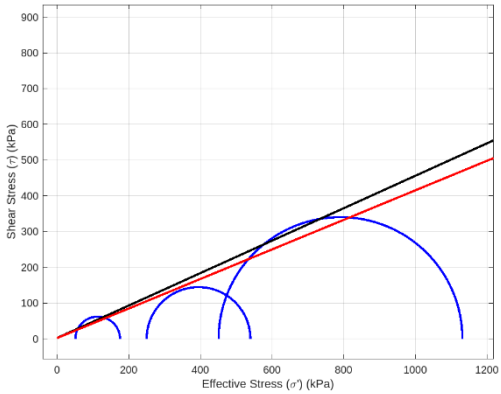

Figure 64: GT-D25-Co.8 effective stress

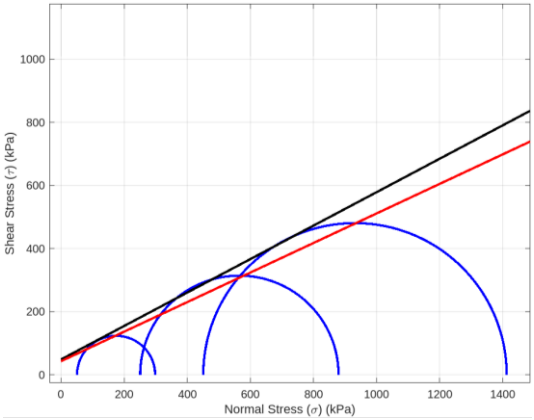

Figure 65: GT-D25-C1.2 total stress

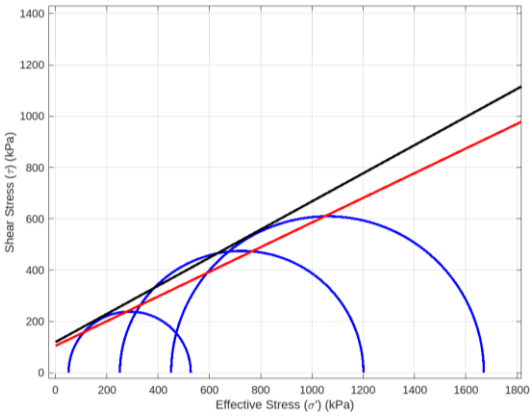

Figure 66: GT-D25-C1.2 effective stress

Appendix B – Gregory's Model to Calculate FRS Properties

GREGORY METHOD OF ESTIMATING SHEAR STRENGTH INCREASE

Notice: This spreadsheet is provided "AS IS" with no warranty, guarantee, or representation as to the accuracy or applicapability of the results. The results must be verified by a professional engineer experienced in FRS applications. By using this spreadsheet, you acknowledge and accept these conditions.

		Input in Blue Cells Only.			PI/180	
Length of Fibers	l	2	inches		0.017453	
Width of Fibers	w	0.1000	inches			
Thickness of Fibers	t	0.00150	inches			
Equivalent Diameter	d	0.01382	inches			
Effective Aspect Ratio	a_{re}	72.36				
Friction angle (effective)	ϕ	24				
Cohesion (effective)	c	6.8893	lb/sq in	992.06	lb/sq ft	
For NC Clay K_o=1-sinϕ	K_o	0.593263		σ_r =	15.47	psi
Constant, K_e						
K_e=(0.75K_o+0.25)	K_e	0.694948				
Friction factor	f_ϕ	0.244	(0.5 maximum unless based on actual interface tests)			
Cohesion factor	f_c	0.3	(0.5 maximum unless based on actual interface tests)			
Weight of fibers	w	0.08	lb/cu ft			
Unit weight of water	γ_w	62.4	lb/cu ft			
Specific gravity of fibers	G_s	0.91	0.91 for PP			
Volume ratio factor	$1/G_s\gamma_w$	0.0176				
Volume ratio	V_r	0.0013				
Change in Friction Angle Due to Fibers	$\Delta\phi_{gm}$	0.4	degrees			
Reinforced Friction Angle	ϕ_{gm}	**24.4**	**degrees**			
Uncorrected Increase in Cohesion Due to Fibers	Δc_{gm}	0.198	lb/sq in	28.44	lb/sq ft	
Reduction in Δc_{gm}		0.134	lb/sq in	19.33	lb/sq ft	
Reinforced Cohesion	c_{gm}	**6.953**	**lb/sq in**	**1001.18**	**lb/sq ft**	

Note: Large fiber content may result in C_{gm} being negative. Set C_{gm} = 0.0 in this case.

Appendix C – HP570 Technical Data Sheet

TECHNICAL DATA SHEET

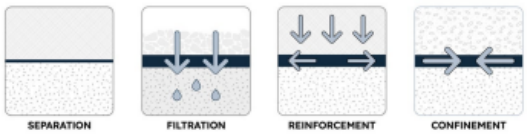

MIRAFI HP570

MIRAFI® HP570 geotextile is composed of high-tenacity monofilament polypropylene yarns, which are woven into a network such that the yarns retain their relative position. MIRAFI HP570 geotextile is inert to biological degradation and resistant to naturally encountered chemicals, alkalis, and acids.

TenCate Geosynthetics Americas (A Solmax Company) is accredited by Geosynthetic Accreditation Institute – Laboratory Accreditation Program (GAI-LAP).

MIRIFI HP570 meets Build America, Buy America Act, Pub. L. No. 117-58, div. G §§ 70901-52.

MECHANICAL PROPERTIES	TEST METHOD	UNIT	MINIMUM AVERAGE ROLL VALUE	
			MD	CD
Tensile Strength (at ultimate)	ASTM D4595	lbs/ft (kN/m)	4800 (70.0)	4800 (70.0)
Tensile Strength (at 5% strain)	ASTM D4595	lbs/ft (kN/m)	2400 (35.0)	3000 (43.8)
Grab Tensile Strength	ASTM D4632	lbs (N)	500 (2225)	500 (2225)
Grab Tensile Elongation	ASTM D4632	%	11	4
Trapezoid Tear Strength	ASTM D4533	lbs (N)	180 (801)	180 (801)
CBR Puncture Strength	ASTM D6241	lbs (N)	2000 (8900)	
			MINIMUM ROLL VALUE	
Flow Rate	ASTM D4491	gal/min/ft² (l/min/m²)	35 (1426)	
Permittivity	ASTM D4491	sec^{-1}	0.5	
			MAXIMUM OPENING SIZE	
Apparent Opening Size (AOS)	ASTM D4751	U.S. Sieve (mm)	30 (0.60)	
			MINUMUM TEST VALUE	
UV Resistance (at 500 hours)	ASTM D4355	% strength retained	80	

PHYSICAL PROPERTIES	UNIT	ROLL SIZE
Roll Dimensions (width x length)	ft (m)	15 x 300 (4.5 x 91)
Roll Area	yd² (m²)	500 (418)
Estimated Roll Weight	lbs (kgs)	400 (182)

365 South Holland Drive Pendergrass, GA 30567
Tel +1 706 693 2226 www.tencategeo.us

SOLMAX